Redox Biology 50 (2022) 102235

Contents lists available at ScienceDirect

Redox Biology

journal homepage: www.elsevier.com/locate/redox

PERK prevents hepatic lipotoxicity by activating the p62-ULK1 axis-mediated noncanonical KEAP1-Nrf2 pathway

Da Hyun Lee [a,b], Jeong Su Park [b], Yu Seol Lee [a,b], Soo Han Bae [a,b,*]

[a] Severance Biomedical Science Institute, Graduate School of Medical Science, Brain Korea 21 Project, Yonsei University College of Medicine, Republic of Korea
[b] Severance Biomedical Science Institute, Yonsei Biomedical Research Institute, Yonsei University College of Medicine, 50 Yonsei-ro, Seodaemun-gu, Seoul, 03722, Republic of Korea

ARTICLE INFO

Keywords:
PERK
KEAP1-Nrf2 pathway
Lipotoxicity
Nonalcoholic steatohepatitis
p62
ULK1

ABSTRACT

Hepatic lipotoxicity is a crucial factor in nonalcoholic steatohepatitis resulting from excessive saturated fatty acid-induced reactive oxygen species (ROS)-mediated cell death, which is associated with the accumulation of endoplasmic reticulum (ER) stress in the liver. The unfolded protein response (UPR) alleviates ER stress by restoring ER protein folding homeostasis. However, whether UPR contributes ROS elimination under lipotoxicity remains unclear. The Kelch like ECH-associated protein 1 (KEAP1)-nuclear factor, erythroid 2 like 2 (Nrf2) pathway provides antioxidant defense against lipotoxic stress by eliminating ROS and can be activated by the p62-Unc-51 like autophagy activating kinase 1 (ULK1) axis. However, the upstream molecular regulator of the p62-ULK1 axis-induced KEAP1-Nrf2 pathway in the same context remains unidentified. Here, we demonstrated that PKR-like ER kinase (PERK), a UPR sensor, directly phosphorylates p62 and ULK1, thereby activating the noncanonical KEAP1-Nrf2 pathway. We also elucidated the molecular mechanism underlying the PERK-mediated p62-ULK1 axis-dependent noncanonical KEAP1-Nrf2 pathway, which could represent a promising therapeutic strategy against hepatic lipotoxicity.

1. Introduction

Hepatic lipotoxicity, caused by excessive cell death mediated by saturated fatty acid (SFA)-induced reactive oxygen species (ROS) production [1,2], is a key pathogenic feature of nonalcoholic steatohepatitis (NASH) [3,4]. Increased oxidative stress, associated with an imbalance between ROS production and antioxidant responses [5], has been observed in the livers of patients with NASH [6,7]. Since there are no pharmacological treatments for NASH at present, it is critical to develop effective therapeutic target strategies to remove oxidative stress.

The nuclear factor, erythroid 2 like 2 (Nrf2) is the key transcription factor that coordinates the elimination of ROS by inducing the expression of antioxidant enzymes in response to oxidative stress and known to protect the liver against NASH [8–11]. Nrf2 is negatively regulated by the suppressor protein, Kelch like ECH-associated protein 1 (KEAP1) [12]. Nrf2 is degraded via the KEAP1-dependent ubiquitin-proteasome pathway under non-stress conditions [8,9,12,13]. However, the cysteine residues in KEAP1 are modified in response to oxidative stress; therefore, Nrf2 can be released from KEAP1 and translocated into the nucleus, where it activates target genes for antioxidant enzymes. This is known as the canonical KEAP1-Nrf2 pathway [8,9]. p62 is an autophagy receptor protein that activates Nrf2 through specific binding to KEAP1 [14,15], which corresponds to the most well-known noncanonical KEAP1-Nrf2 pathway [16]. Furthermore, S351-phosphorylated p62 has a higher affinity for KEAP1, which corresponds to strong Nrf2 activation [15,17]. Moreover, p62-mediated Nrf2 activation can be induced by autophagic KEAP1 degradation [13].

Endoplasmic reticulum (ER) stress, resulting from the accumulation of unfolded or misfolded proteins in the ER [18], manifests high in the livers of patients with NASH [19–21]. ER stress has been suggested to be promoted by excessive quantities of SFA through an increase in the synthesis of ceramide, an important building block in sphingolipids, which disrupts ER homeostasis [22,23]. It decreases the sarco/ER Ca^{2+}-ATPase activity and leads to Ca^{2+} leakage, which attenuates the mitochondrial electron transport chain and enhances mitochondrial

Abbreviations: GFP, green fluorescent protein; HCD, high-carbohydrate diet; ALT, alanine aminotransferase; BSA, bovine serum albumin; IHC, immunohistochemistry; GST, glutathione S-transferase; Grp78, glucose regulatory protein 78; 3NT, 3-nitrotyrosine; 4HNE, 4-hydroxynonenal.

* Corresponding author. Severance Biomedical Science Institute, Yonsei University College of Medicine, 50-1 Yonsei-ro, Seodaemun-gu, Seoul, 03722, Republic of Korea.
E-mail address: soohanbae@yuhs.ac (S.H. Bae).

https://doi.org/10.1016/j.redox.2022.102235
Received 16 November 2021; Received in revised form 16 December 2021; Accepted 12 January 2022
Available online 14 January 2022

Abbreviations

3NT	3-nitrotyrosine
4HNE	4-hydroxynonenal
ACTB	actin beta
ALT	alanine aminotransferase
AMPK1/2	protein kinase AMP-activated catalytic subunits alpha1/2
ATF6	activating transcription factor 6
BafA1	bafilomycin A1
BSA	bovine serum albumin
CM-H2DCFDA	5-(and-6)-chloromethyl-2′,7′-dichlorodihydrofluorescein diacetate
ER stress	endoplasmic reticulum stress
GFP	green fluorescent protein
Grp78	glucose regulatory protein 78
GST	glutathione S-transferase
GSTA1	glutathione S-transferase A1
HCD	high-carbohydrate diet
HMOX1/HO-1	heme oxygenase 1
IHC	immunohistochemistry
IRE1	inositol-requiring enzyme 1
KEAP1	kelch like ECH associated protein 1
LC3B	microtubule-associated protein 1 light chain 3
MEF	mouse embryonic fibroblast
NAFLD	nonalcoholic fatty liver disease
NASH	nonalcoholic steatohepatitis
Nrf2	nuclear factor, erythroid 2 like 2
NQO1	NAD(P)H quinone dehydrogenase 1
p62	Sequestosome 1
PA	palmitic acid
PARP	poly (ADP-ribose) polymerase 1
PERK	PKR-like ER kinase
ROS	reactive oxygen species
SFA	saturated fatty acid
siRNA	small interfering RNA
TUNEL	terminal deoxynucleotidyl transferase-mediated dUTP nick-end labeling
ULK1	unc-51 like autophagy activating kinase
UPR	unfolded protein response

fatty acid oxidation, which is followed by ROS generation and cell death [3,4,7]. ER stress manifests through the activation of the unfolded protein response (UPR) pathway, which has three major stress sensors: inositol-requiring enzyme 1 (IRE1), PKR-like ER kinase (PERK), and activating transcription factor 6 (ATF6) [24]. The chaperone GRP78, a repressor of UPR stress sensors, is dissociated from these three transducers (IRE1, PERK, and ATF6); it controls the adaptive responses and protects cells against ER stress by suppressing translation and inducing the degradation of misfolded proteins [25]. However, whether UPR regulates the elimination of ROS in response to lipotoxicity has not been explored.

In this study, we demonstrated that PERK, one of the UPR sensors, plays a protective role in lipotoxicity through Unc-51 like autophagy activating kinase 1 (ULK1)-induced autophagic KEAP1 degradation and phosphorylation of the p62-mediated noncanonical KEAP1-Nrf2 pathway. We also elucidated the molecular mechanism and physiological relevance of lipotoxicity *in vivo*.

2. Materials and methods

2.1. Mice and in vivo transfection

All animal experiments were approved by the Animal Care and Use Committee of the Yonsei University College of Medicine. Male C57BL/6J mice (B6, [SLC-M-0133]) aged 8 weeks were used in the animal experiments, which is purchased from Japan SLC, Inc. (Hamamatsu, Japan). All mice had free access to water and food and were housed in cages maintained at 23 ± 2 °C under a 12 h light/12 h dark cycle and 50%–70% humidity. To the depletion of PERK in mice, *PERK* siRNA (20 nM, Santa Cruz Biotechnology; sc-36214) was injected through the tail vein along with the Invivofectamine 3.0 reagent (Thermo Fisher Scientific, IVF3001) for 3 days according to the manufacturer's instructions. Mice were fed a normal chow diet (LabDiet, 5053) without fasting or a high-carbohydrate diet (HCD; Dyets, 102235) after 24 h of fasting. After 18 h of refeeding, the mice were sacrificed. The serum alanine aminotransferase (ALT) levels were measured via colorimetric determination using an activity assay kit (FUJIFILM, 3250).

2.2. Cell lines

HEK293 cells (Korean Cell Line Bank, 21573), mouse embryonic fibroblasts (MEFs), and green fluorescent protein (GFP)-conjugated LC3B (GFP-LC3B)-expressing HeLa (GFP-LC3B HeLa) cells were maintained in Dulbecco's modified Eagle's medium (DMEM; Hyclone, HS3243.01) supplemented with 10% fetal bovine serum (Hyclone, SV30087.02) and 1% penicillin-streptomycin (Biowest, L0022) in a 5% CO_2 atmosphere at 37 °C. Hepa1c1c7 cells (Korean Cell Line Bank, 22026) were maintained in minimum essential media (Welgene, LM007-01) supplemented with 10% fetal bovine serum and 1% penicillin-streptomycin in a 5% CO_2 atmosphere at 37 °C. *PERK* MEFs was kindly provided by Dr. S. H. Back (University of Ulsan, Republic of Korea). GFP-LC3B HeLa cells were provided by Dr. M.J. Lee (Seoul National University, College of Medicine, Republic of Korea).

2.3. Immunoblot analysis

For immunoblot analysis, the cells were lysed in lysis buffer containing 50 mM tris-HCl (pH 7.5), 150 mM NaCl, aprotinin, leupeptin, and 1% Nonidet P-40 (NP-40). Cell lysates were centrifuged (13,500 rpm for 15 min), and the resulting supernatants were subjected to sodium dodecyl sulfate polyacrylamide gel electrophoresis (SDS-PAGE); the separated proteins were transferred to polyvinylidene fluoride membranes (PVDF; MERK Millipore IPVH00010). After blocking with 5% skim milk in Tris-buffered saline and 0.1% Tween 20 (TBS-T), the membranes were then incubated with the specific primary antibodies at 4 °C overnight, followed by incubation with horseradish peroxidase-conjugated secondary antibodies at room temperature for 1 h. The proteins were visualized using an enhanced chemiluminescence solution (Thermo Scientific, 34580).

2.4. Antibodies and reagents

The following antibodies were used in this study: anti-KEAP1 (Proteintech, 10503-2-AP); anti-ACTB (Santa Cruz Biotechnology, sc-47778); anti-FLAG (Merk Millipore, F1804); anti-p-ULK1 (S317) (Cell Signaling Technology, 12753S); anti-ULK1 (Sigma Aldrich, A7481); anti-p62 (Abnova, H00008878-M01); anti-p-p62 (S351) (gift from Dr. Rhee SG and Komatsu); anti-LC3B (Novus, NB100-2220); anti-MYC (Merk Millipore, 05-419); anti-AMPK (Cell Signaling Technology, 2603); anti-cleaved CASP3 (Cell Signaling Technology, 9661S); anti-cleaved PARP (Cell Signaling Technology, 9544S); anti-Nrf2 (Santa Cruz Biotechnology, sc-13032); anti-LaminB (Proteintech, 12987-1-AP); anti-HA (Bethyl Laboratory, A190-108A); anti-GFP (Santa Cruz Biotechnology, sc-9996); anti-PERK (Santa Cruz Biotechnology; sc-

377400); anti-p-PERK (T980) (Cell Signaling Technology, 3179S), anti-p-eIF2 alpha (S51) (Cell Signaling Technology, 9721S); anti-eIF2 alpha (Enzo Life Sciences, ADI-KAP-CP130); anti-p-IRE1 alpha (S724) (Thermo Fisher Scientific, PA1-16927); anti-IRE1 alpha (Novus biologicals, NB100-2324); anti-GRP78 (BD Biosciences, BD 610979); anti-ATF6 (Abcam, AB11909); anti-ATF4 (Santa Cruz Biotechnology, sc-11815); anti-GST (abm, G018). PA (Sigma Aldrich, 57-10-36), DMSO (Sigma Aldrich, 67-68-5), bafilomycin A1 (BafA1; Sigma Aldrich, B1793), GSK2656157 (Sellectchem, S7033), LysoTracker Green (Thermo Fisher Scientific, L7526), and ERTracker Red (Invitrogen, E34250) were used.

2.5. Saturated fatty acid (SFA) treatment

Palmitic acid (PA) was dissolved in isopropyl alcohol at a stock concentration of 160 mM. For the treatment of saturated fatty acid (SFA), the cells were incubated with PA (500 μM) DMEM containing 1% bovine serum albumin (BSA) for 18 h to ensure a physiologically suitable ratio between the bound and unbound free fatty acids in the medium [26–29].

2.6. MTT assay for cell viability

Cells were seeded at 2×10^3 cells/well in a final volume of 100 μL in 96-well plates. After 24 h, the cells were treated with BSA, PA (500 μM), or 4-phenylbutyric acid (4-PBA) for the indicated durations. Cell viability was detected using a CellTiter-Glo luminescent cell viability assay kit (Promega Corporation, G7570) according to the manufacturer's instructions.

2.7. Measurement of reactive oxygen species (ROS) levels

Intracellular ROS generation was assessed using 5,6-chloromethyl-2,7-dichlorodihydrofluorescein diacetate (CM-H2DCFDA; Molecular Probes, Eugene, OR, USA). Cells (3×10^5) were plated in 35 mm dishes. After 24 h, the cells were treated with BSA or PA, and then with PBA, for the indicated durations, rinsed once with 2 mL Hank's balanced salt solution (HBSS), and incubated for 5 min with CM-H_2DCFDA. The cells were washed again with HBSS, and images were obtained using a fluorescence microscope (Olympus, IX73). The relative dichlorofluorescein fluorescence was calculated by averaging the levels of fluorescence in 80–100 cells after subtracting the background fluorescence.

2.8. Subcellular fractionation

Cells or liver tissues were lysed in a cytoplasmic extraction reagent containing 10 mM HEPES (bioWORLD, 40820042-1), 1.5 mM $MgCl_2$, 10 mM KCl, 0.5 mM dithiothreitol (DTT) (Sigma Aldrich, 10197777001), 0.05% of 0.5% IGEPAL® CA-630 (Sigma Aldrich, 56741), PMSF (Sigma Aldrich, 10837091001), 1 mg/mL aprotinin and 1 mg/mL leupeptin. The lysates were centrifuged (900×*g* for 10 min) at 4 °C, and the pellet was resuspended in a nuclear extraction reagent (containing 5 mM HEPES (pH 8.0), 0.2 mM EDTA, 1.5 mM $MgCl_2$, 0.5 mM DTT, and 26% glycerol) on ice. The lysates were then centrifuged (24,000×*g* for 20 min) at 4 °C, and the supernatants were subjected to immunoblot analysis using Nrf2 and LMNB1 (nuclear protein marker) antibodies.

2.9. Small interfering RNA (siRNA) transfection

GFP-LC3B HeLa cells were transfected with siRNAs targeting PERK (20 nM, Santa Cruz Biotechnology; sc-36213) or control siRNA (20 nM, Bioneer; SP-1011). Hepa1c1c7 cells were transfected with siRNAs targeting PERK (20 nM, Santa Cruz Biotechnology; sc-36214) or control siRNA (20 nM). The cells were transfected with siRNAs using Lipofectamine RNA/iMAX, according to the manufacturer's instructions (Invitrogen, P/N 56532).

2.10. Quantitative RT-PCR analysis

Total RNA was prepared from cultured cells using TRIzol® reagent (MRC, TR 118) and treated with RNase (Sigma Aldrich, R6148). Total RNA (1 μg) was then subjected to reverse transcription with random hexamer primers using a TAKARA cDNA synthesis kit (TaKaRa, RR036A). The resulting cDNA was subjected to quantitative PCR analysis using SYBR® Green (ABI, 4367659) and mouse- and human-specific primer pairs (forward and reverse, respectively). The sequences of the primers used for cDNA were as follows (Table S1).

2.11. Histological and immunohistochemistry (IHC) analysis

The liver tissues of mice were fixed in 10% neutral-buffered formalin solution (Sigma Aldrich, HT501128) embedded in paraffin, and sectioned into slices of 5-μm. The liver sections were subjected to hematoxylin and eosin (H&E) staining and IHC analysis with antibodies against 4-hydroxynonenal (4-HNE; JaICA, MHN-100P) or 3-nitrotyrosine (3-NT; Merck Millipore, 06–284). Images were obtained by using a fluorescence microscope (Olympus, BX43).

2.12. Terminal deoxynucleotidyl transferase-mediated dUTP nick-end labeling (TUNEL) analysis

To evaluate apoptosis in mouse livers, MEFs, and Hepa1c1c7 cells, TUNEL assay kit (Promega, Madison, WI, USA) was used according to the manufacturer's instructions. Fluorescence signals were detected using a confocal microscope (Carl Zeiss, LSM 700). The frequency of detection of apoptotic cells in the liver sections or the cells was measured by determining the percentage of TUNEL-positive cells in five random microscopic fields per specimen.

2.13. Immunofluorescence analysis

To analyze the GFP puncta, GFP-LC3B HeLa cells were cultured on glass plates in 12-well plates. The cells were washed with Dulbecco's phosphate-buffered saline (Biowest, X0515-500), fixed with 4% paraformaldehyde (Biosesang, P2031) for 30 min, and washed three times with PBS. To analyze the autolysosomes, MEFs were stained with LysoTracker Green DND-26 (Thermo Fisher Scientific, L7526), according to the manufacturer's instructions. Hepa1c1c7 cells were stained with ERTracker Red (Invitrogen, E34250) according to the manufacturer's instructions. To perform the proximity ligation assay (PLA), Duolink II PLA probes (Olink Bioscience, DUO92001 and DUO92005) and detection reagents (Olink Bioscience, DUO92014) were used according to the manufacturer's instructions. The nuclei were counterstained with DAPI, and the PLA and fluorescence signals were detected using a confocal microscope (Carl Zeiss, LSM 700).

2.14. Protein purification and in vitro kinase assay

Glutathione *S*-transferase (GST)-tagged recombinant p62 and GST-ULK1 proteins were purified from bacteria using GST Sepharose beads according to the manufacturer's instruction (GE Healthcare). GST-p62 cDNAs were kindly provided by Dr. T. Johansen (University of Tromsø, Norway). GST-ULK1 cDNAs were kindly provided by Dr. S-W Yu (Daegu Gyeongbuk Institute of Science and Technology [DGIST], Republic of Korea). HEK293 cells transfected with MYC-PERK WT, MYC-PERK kinase dead (K618A) were subjected to immunoprecipitation using a mouse anti-MYC antibody for 4 h at 4 °C, followed by overnight incubation at 4 °C with G-Sepharose beads. The next day, the kinase reaction was initiated by treating with 200 μM ATP and recombinant GST-p62 or GST-ULK1 proteins for 40 min at 37 °C. The kinase reaction buffer was composed of 20 mM Tris-HCl, 10 mM MgCl2, 5 mM DTT, and 0.4 mM NaF at pH 7.2–7.5. The reaction was terminated by adding sodium dodecyl sulfate sample buffer and boiling for 10 min at 100 °C. The

samples were subjected to immunoblot analysis using anti-phospho-p62 (S351) and anti-phospho-ULK1 (S317).

2.15. GST pull-down assay

MYC-PERK was prepared via *in vitro* translation using a TNT-coupled SP6 reticulocyte lysate system (Promega, L4600). Pull-down assays were performed by incubating equal quantities of GST or GST-p62, and ULK1 fusion proteins were immobilized onto glutathione-Sepharose beads (GE Healthcare Bio-sciences) [30,31]. The mixture containing *in vitro* translated MYC-PERK was placed on a rocking platform for 1 h and, washed three times with a washing buffer (composed of 20 mM Tris-HCl (pH 8.0), 150 mM NaCl, and 0.5% Nonidet P-40), and the bound proteins were eluted and separated by 8% SDS-PAGE. MYC-PERK was detected via immunoblot analysis using an anti-MYC antibody.

2.16. Statistical analysis

Data were analyzed using two-tailed Student's t-tests for comparisons between two groups or one-way analysis of variance (ANOVA) with Tukey's test for comparing three or more groups using Prism 9.0 (GraphPad, La Jolla, CA, USA) software to determine statistical significance. A value of $P < 0.05$ was considered significant.

3. Results

3.1. Activation of the p62-mediated noncanonical KEAP1-Nrf2 pathway is dependent on ER stress in response to lipotoxicity

Saturated fatty acids (SFAs) induce ER stress and oxidative stress-mediated cell death, which is known as lipotoxicity [4,32–34]. To assess the p62-mediated activation of the noncanonical KEAP1-Nrf2 pathway in response to lipotoxicity, we treated Hepa1c1c7 cells and mouse embryonic fibroblasts (MEFs) with palmitic acid (PA), which is the most common SFA found in humans [35]. Hepa1c1c7 cells, mouse hepatoma cell line, are a suitable *in vitro* model for study of liver disease, because that can express liver phenotypes in cultured conditions [19]. MEFs, generated from a genetically manipulated mouse embryo, can be used to investigate molecular mechanisms of protein functions and cellular signaling [18]. Our results showed that PA increased the p62 phosphorylation at S351, p62 expression, and autophagic KEAP1 degradation, followed by activation of Nrf2 target genes including *p62*, *GSTA1*, and *HO-1* in time dependent manner in both Hepa1c1c7 cells (Fig. S1A-G) and MEFs (Fig. S1K-Q). Especially, this p62-mediated noncanonical KEAP1-Nrf2 pathway was dramatically activated in the both cells treated with PA for 18 h. Moreover, we observed that accumulation of ER stress was increased under lipotoxic conditions at the same time by detecting the increase of expression levels of the ER stress marker glucose regulatory protein 78 (Grp78) and ER stress target genes (such as *Grp78*, *Atf4*, and Trb3) in Hepa1c1c7 cells (Fig. S1A, Fig. S1H–S1J) and MEFs (Fig. S1K, S1R-S1T). It is known that unfolded protein response (UPR) pathway plays protective roles against ER stress [2]. The activation of the UPR pathway depends on the three stress sensors [36]. To determine whether the UPR pathway is also associated with lipotoxic conditions, we measured the levels of these three UPR sensors, including PKR-like ER kinase (PERK), inositol-requiring enzyme 1 alpha (IRE1α), and activating transcription factor 6 (ATF6) in response to PA. We found that the phosphorylation of PERK was increased drastically in the both cells (Figs. S1A and S1K). Therefore, we carried out the PA treatment in both Hepa1c1c7 cells and MEFs to induce SFA-mediated ER stress and lipotoxicity.

To verify whether the activation of p62-mediated noncanonical KEAP1-Nrf2 pathway is regulated by SFA-mediated ER stress, we treated Hepa1c1c7 cells with 4-phenylbutyric acid (4-PBA), an ER stress inhibitor [37], under lipotoxic conditions. We found that the inhibition of ER stress prevented the accumulation of p62 and its phosphorylated form (S351) as well as the autophagic degradation of KEAP1, thereby suppressing Nrf2 target genes, including *Gsta1*, *HO-1*, and *Nqo1* (Fig. 1A–G). Moreover, SFA-induced cell death was restored upon the inhibition of ER stress, as measured in the terminal deoxynucleotidyl transferase-mediated dUTP nick-end labeling (TUNEL) (Fig. 1H–I) and MTT assays (Fig. 1J). We also found that SFA-induced ROS accumulation was partly blocked after PBA treatment under lipotoxic conditions (Fig. 1K–L).

To determine whether the p62-mediated noncanonical KEAP1-Nrf2 pathway was associated with the UPR pathway, we measured the levels of these three UPR sensors in Hepa1c1c7 cells treated with PBA under lipotoxic conditions. Interestingly, we found that the phosphorylation of PERK was increased in the SFA-treated cells but was dramatically downregulated upon the inhibition of ER stress (Fig. 1M-N, 1Q). The levels of IRE1α phosphorylation and cleaved ATF6 were not significantly different in the same context, which is consistent with findings from other reports [38–43] (Fig. 1M). Furthermore, the expression levels of the ER stress marker glucose regulatory protein 78 (Grp78) and ER stress target genes (such as *Grp78*, *Trb3*, and *Atf4)* were reduced after PBA treatment in response to lipotoxicity (Fig. 1M, 1O–S). Taken together, these results demonstrate that the p62-mediated noncanonical KEAP1-Nrf2 pathway is activated in an ER stress-dependent manner in response to lipotoxicity.

3.2. PERK directly phosphorylates p62 at S351 and activates the noncanonical KEAP1-Nrf2 pathway, thereby protecting cells against lipotoxicity

To determine whether PERK, which is primarily activated by PA-mediated ER stress, is required for the activation of the p62-mediated noncanonical KEAP1-Nrf2 pathway, we transfected Hepa1c1c7 cells with *PERK* small interfering RNA (siRNA), and then treated with PA (Fig. S2A). We found that the induction of p62 and its phosphorylation at S351 were abruptly blocked in si*PERK*-mediated knockdown Hepa1c1c7 cells, resulting in the inhibition of Nrf2 activation in response to lipotoxicity (Fig. S2A-S2F). Furthermore, to verify whether this pathway is mediated by PERK, we treated *PERK* wild type (WT) or *PERK* knock out (KO) MEFs with PA. We showed that the increase of S351-phosphorylated p62 and p62 was drastically inhibited in the *PERK* KO MEFs under lipotoxic conditions, followed by blockage of Nrf2 activation (Fig. 2A-E). To examine how PERK activates the p62-mediated noncanonical KEAP1-Nrf2 pathway, we investigated whether PERK can directly phosphorylate p62 as a kinase protein. First, the results of the glutathione S-transferase (GST) pull-down assay provided evidence that p62 directly binds to PERK (Fig. 2J). To verify whether PERK can act as a direct kinase of p62 for phosphorylation at the S351 site, we purified GST-p62 and performed an *in vitro* kinase assay using the MYC-PERK WT or MYC-PERK kinase-dead mutant (KD, K618A) vectors. We transfected HEK293 cells with MYC-PERK WT or KD, and subjected the cell lysates to co-immunoprecipitation analysis using an anti-MYC antibody. Recombinant GST-p62 was incubated with the PERK immune complex in the absence or presence of ATP. We found that MYC-PERK WT phosphorylated GST-p62, whereas MYC-PERK KD (K618A) did not mediate the phosphorylation of GST-p62 at S351 in the presence of ATP (Fig. 2K–L). To further verify whether PERK mediates the direct phosphorylation of p62 in response to lipotoxicity, we transfected *PERK* KO MEFs with MYC-PERK WT or MYC-PERK KD (K618A) and treated these cells with PA. p62 phosphorylation at S351 increased in the MYC-PERK WT-transfected cells under lipotoxicity, whereas it decreased in the MYC-PERK KD-transfected cells (Fig. 2M-N). Collectively, these findings demonstrate that PERK exhibits direct kinase activity in phosphorylating p62 at S351.

Moreover, we found that PERK plays a protective role against lipotoxicity, as evaluated through the MTT and TUNEL assays (Fig. 2O–Q and S2I–S2K). We showed that the expression levels of cell death markers, such as cleaved poly(ADP-ribose) polymerase (PARP) and

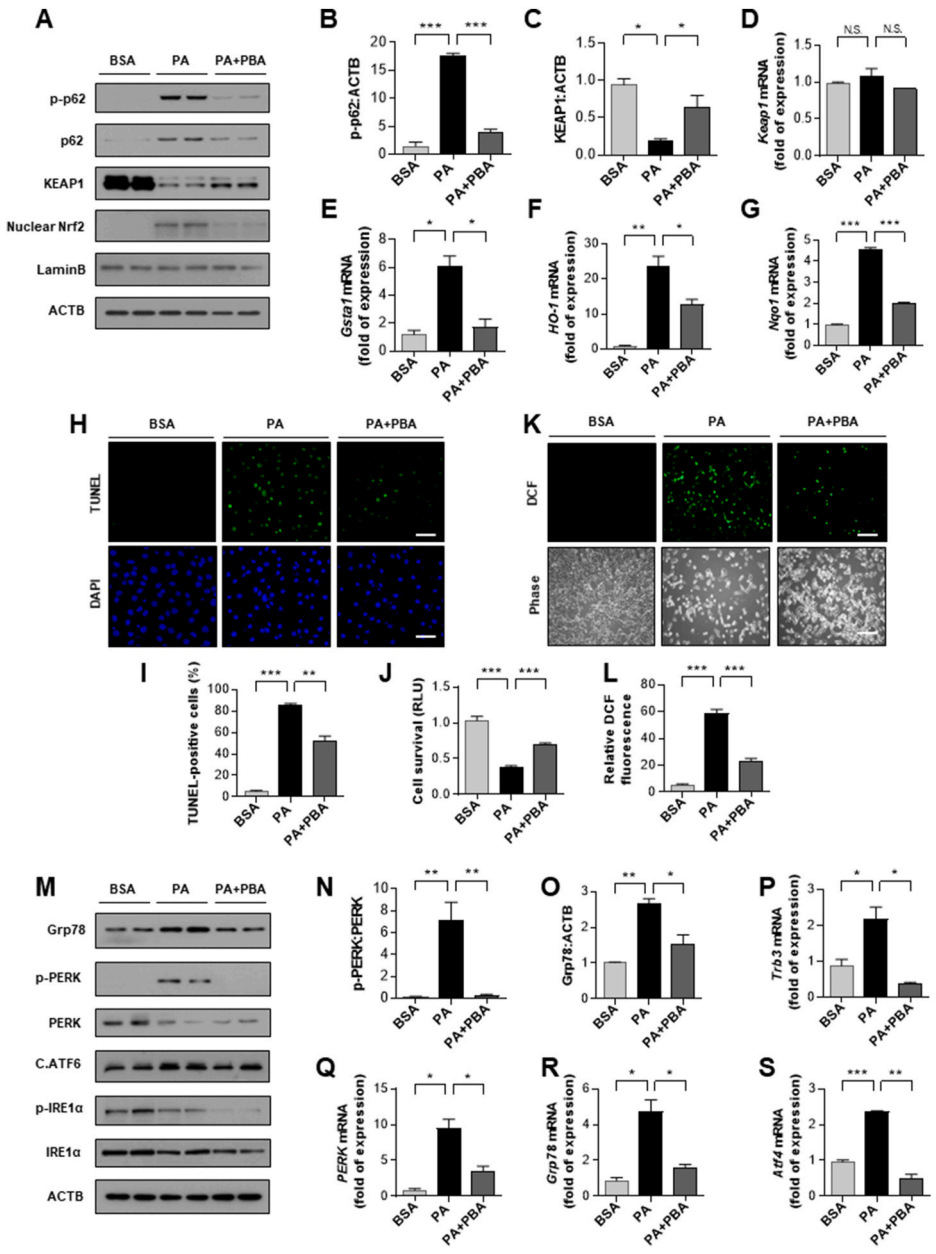

Fig. 1. Activation of the p62-mediated noncanonical KEAP1-Nrf2 pathway is dependent on endoplasmic reticulum (ER) stress and protects cells against lipotoxicity. Hepa1c1c7 cells were treated with palmitic acid (PA; 500 μM) and 4-phenylbutyric acid (4-PBA; 1 mM) for 18 h. (**A**) Immunoblot analysis using antibodies against p-p62 (S351), p62, KEAP1, nuclear Nrf2, LaminB (nucler protein marker), and ACTB (loading control). (**B, C**) Densitometric analysis of the immunoblots. Quantitative RT-PCR (qRT-PCR) analysis of *Keap1* (**D**), *Gsta1* (**E**), *HO-1* (**F**), and *Nqo1* (**G**) mRNA. (**H–I**) Terminal deoxynucleotidyl transferase-mediated dUTP nick-end labeling (TUNEL) analysis of cells treated as described in (**A**). Scale bar: 100 μm. (**I**) Quantitative analysis of TUNEL-positive cells. (**J**) Cell viability was evaluated using a Cell Titer-Glo assay kit. The number of live cells have expression as absorbance at luminescence. (**K**) The levels of reactive oxygen species (ROS) were determined using CM-H2DCFH-DA. Scale bar: 100 μm. (**L**) Quantitative analysis of relative DCF fluorescence. (**M**) Immunoblot analysis of cells that were treated as described in (**A**) using antibodies against Grp78, p-PERK, PERK, cleaved ATF6 (C.ATF6), p-IRE1α, IRE1α, and ACTB (loading control). (**N–O**) Densitometric analysis of the immunoblots. qRT-PCR analysis of *Trb3* (**P**), *PERK* (**Q**), *Grp78* (**R**), and *Atf4* (**S**) mRNA. Graphical and statistical analyses were performed using GraphPad Prism 9 software. Bar graphs were drawn using the mean values of the results per sample but the statistical significances were derived from raw data. Data are presented as means ± SD from 3 independent experiments. $^{*}p < 0.05$, $^{**}p < 0.01$, $^{***}p < 0.001$, and N.S., not significant. See also Fig. S1.

caspase-3 (CASP3) are increased in *PERK* KO MEFs (Fig. 2A, 2F-G) and si*PERK*-mediated knockdown Hepa1c1c7 cells (Fig. S2A, S2G-S2H). We also showed that the PERK-induced activation of the p62-mediated noncanonical KEAP1-Nrf2 pathway attenuates PA-induced ROS accumulation (Fig. 2R-S, S2L-S2M), further decreasing the expression levels of ER stress target genes (Fig. 2H–I).

To further confirm whether PERK induces the phosphorylation of p62, we treated Hepa1c1c7 cells with a PERK inhibitor (GSK2656157) [44,45] and incubated them in the absence or presence of PA. We observed that the PERK-mediated phosphorylation of p62 was significantly inhibited, resulting in the blockade of Nrf2 activation in PERK-inactivated cells, and thereby accelerating PA-induced cell death (Fig. S2N–S2T).

Collectively, these results suggest that PERK is required for the activation of the p62-mediated noncanonical KEAP1-Nrf2 pathway by direct phosphorylating p62 at S351, which helps protect cells against lipotoxicity.

3.3. PERK enhances the interaction between AMPK and p62, followed by p62 phosphorylation

Our previous study showed that p62 can be phosphorylated by AMPK (AMP-activated protein kinase) via direct binding [20]. Consistent with previous study [17], we confirmed that p62 physically interacted with AMPK as evidenced by the results of the glutathione S-transferase (GST) pull-down assay (Fig. S3A). Next, we subjected a purified GST-p62 to *in vitro* kinase assay using either the MYC-AMPK wild-type (WT) or kinase-dead mutant (KD, D157A) [46]. Results showed that wild-type AMPK phosphorylated GST-p62 at S351, whereas the catalytically dead mutant of AMPK did not mediate the phosphorylation of GST-p62 (Fig. S3B).

Accordingly, to examine whether PERK induces p62 phosphorylation through the AMPK-p62 axis, we transfected HEK293 cells with HA-p62 and MYC-AMPK expression vectors. Consistent with our previous results, we showed that ectopic expression of AMPK increased the phosphorylation of p62 (Fig. 3A–B). Furthermore, we showed that AMPK-mediated p62 phosphorylation was significantly blocked in both *PERK*

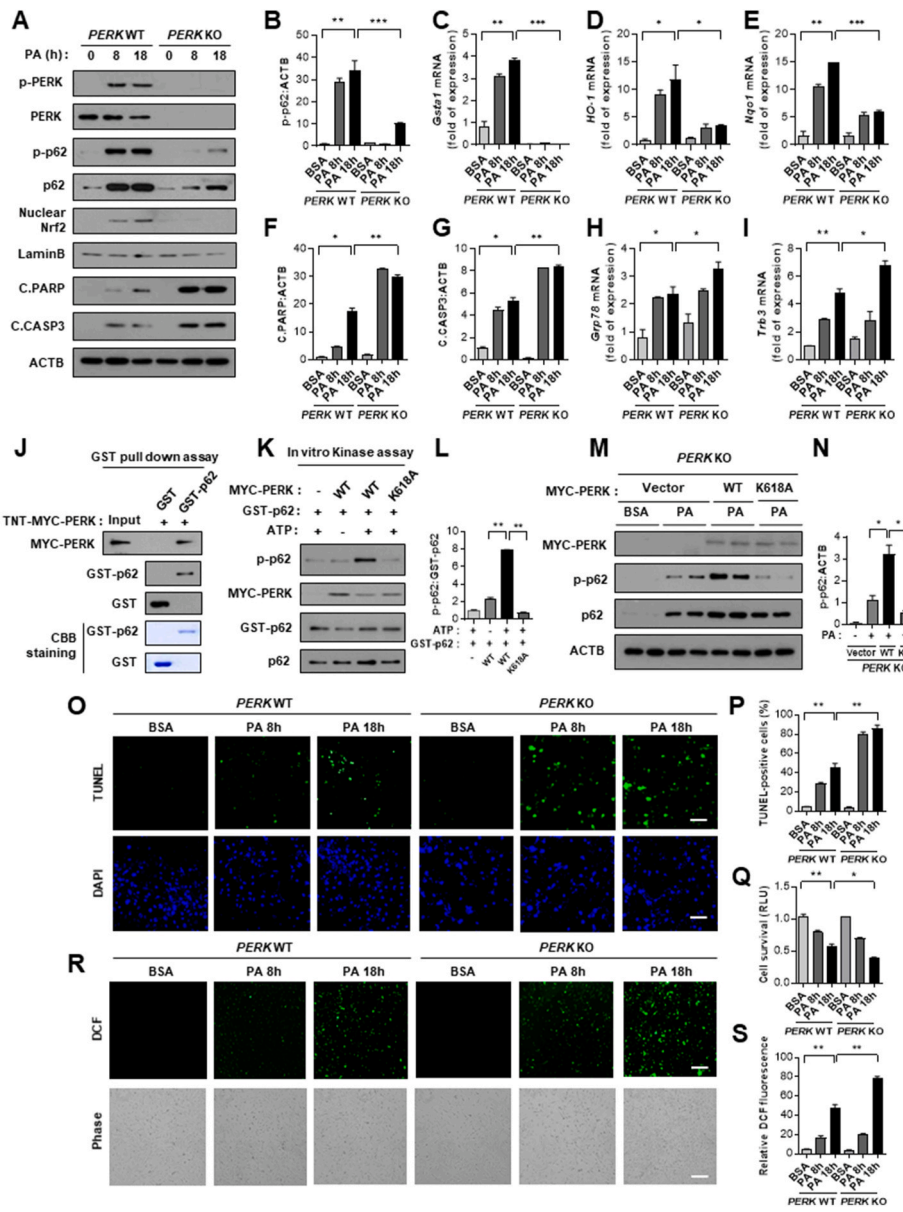

Fig. 2. PERK directly phosphorylates p62 at S351 followed by the activation of the noncanonical KEAP1-Nrf2 pathway, which protects cells against lipotoxicity. (**A**) *PERK* wild-type (WT) or *PERK* knockout (KO) mouse embryonic fibroblasts (MEFs) were treated with palmitic acid (PA) (500 μM) for the indicated durations. Immunoblot analysis using antibodies against p-PERK, PERK, p-p62, p62, nuclear Nrf2, LaminB (nucler protein marker), cleaved PARP (C.PARP), cleaved CASP3 (C.CASP3), and ACTB (loading control). (**B, F-G**) Densitometric analysis of the immunoblots. qRT-PCR analysis of *Gsta1* (**C**), *HO-1* (**D**), *Nqo1* (**E**), *Grp78* (**H**), and *Trb3* (**I**) mRNA. (**J**) *In vitro* translated MYC-PERK was subjected to GST pull-down assays using affinity-purified GST or GST-p62. The proteins bound to GST-p62 were analyzed via immunoblotting with an anti-MYC antibody. The acrylamide gels stained with Coomassie Brilliant Blue (CBB) contained GST and GST-p62 used in the pull-down assay. (**K**) *In vitro* kinase assay for evaluation of p62 phosphorylation at S351. GST or GST-p62 were used as substrates for MYC-PERK WT or K618A (kinase dead mutant) immunoprecipitated from HEK293 cells. Western blotting analysis was performed using S351 phospho-specific antibodies, as well as MYC, GST, and p62 antibodies. (**L**) Densitometric analysis of the immunoblot. (**M**) *PERK* KO MEFs were transfected with MYC-PERK WT or K618A, treated with PA (500 μM) for 18 h, and subjected to immunoblot analysis against MYC, p-p62, p62, and ACTB (loading control). (**N**) Densitometric analysis of the immunoblot. (**O**) Terminal deoxynucleotidyl transferase-mediated dUTP nick-end labeling (TUNEL) analysis of cells treated as described in (**A**). Scale bar: 100 μm. Quantitative analysis of TUNEL-positive cells (**P**) and cell viability (**Q**). (**R**) ROS levels were measured using CM-H_2DCFH-DA. Scale bar: 100 μm. (**S**) Quantification of relative DCF fluorescence. Graphical and statistical analyses were performed using GraphPad Prism 9 software. Bar graphs were drawn using the mean values of the results per sample but the statistical significances were derived from raw data. Data are presented as means ± SD from 3 independent experiments. $^{*}p < 0.05$, $^{**}p < 0.01$, and $^{***}p < 0.001$. See also Fig. S2. (For interpretation of the references to color in this figure legend, the reader is referred to the Web version of this article.)

KO MEFs (Fig. 3C–D) and *PERK*-knockdown Hepa1c1c7 cells (Fig. S3C–S3D). Moreover, we found that MYC-PERK bound to both protein kinases AMP-activated catalytic subunits alpha1/2, (HA-AMPK) (Fig. 3E) and FLAG-p62 (Fig. 3F) in HEK293 cells. We also showed that MYC-PERK interacted with MYC-p62 in the absence of a specific binding domain (Figs. 3G and S3E) in HEK293 cells. Also, co-localization on the ER surface of AMPK-PERK and p62-PERK was measured via confocal microscopy analysis using an ER tracker in Hepa1c1c7 cells (Fig. 3H–I).

To explore whether PERK is involved in the interaction between p62 and AMPK, we transfected HEK293 cells with FLAG-p62 and HA-AMPK expression vectors together with MYC-PERK and subjected the cell lysates to immunoprecipitation (IP) analysis. Results showed that PERK enhanced the binding of p62 and AMPK (Fig. 3J–K).

We further showed that endogenous PERK bound to AMPK (Fig. 3L) and p62 (Fig. 3M) in Hepa1c1c7 cells. Furthermore, we investigated the spatial proximity of endogenous PERK to AMPK and to p62 on the ER following stimulation using an *in situ* proximity ligation assay (PLA), which permits visualization of the spatial proximity of the two proteins. Interestingly, we observed that the PERK-AMPK and PERK-p62 complexes were co-localized in the perinuclear-aggregated ER in Hepa1c1c7 cells (Fig. 3N–P).

To evaluate the association between PERK and the p62-AMPK complex, we examined these interactions in *PERK* WT or *PERK* KO MEFs. The results demonstrated that binding of the p62-AMPK complex was significantly diminished in *PERK* KO MEFs (Fig. 3Q–R). Furthermore, we observed that the endogenous PERK-p62-AMPK complex strongly interacted in PA-treated Hepa1c1c7 cells (Fig. 3S–T). These results indicate that PERK mediates p62 phosphorylation by enhancing the interaction between p62 and AMPK.

3.4. PERK induces autophagy activation, followed by autophagic KEAP1 degradation in response to lipotoxicity

To determine whether PERK is associated with autophagic KEAP1 degradation in response to lipotoxicity, we treated *PERK* WT or *PERK* KO MEFs with PA. Autophagic KEAP1 degradation and the increase in LC3B-II expression were blocked in PA-treated *PERK* KO MEFs (Fig. 4A–D). In addition, to verify the PERK-induced autophagic KEAP1

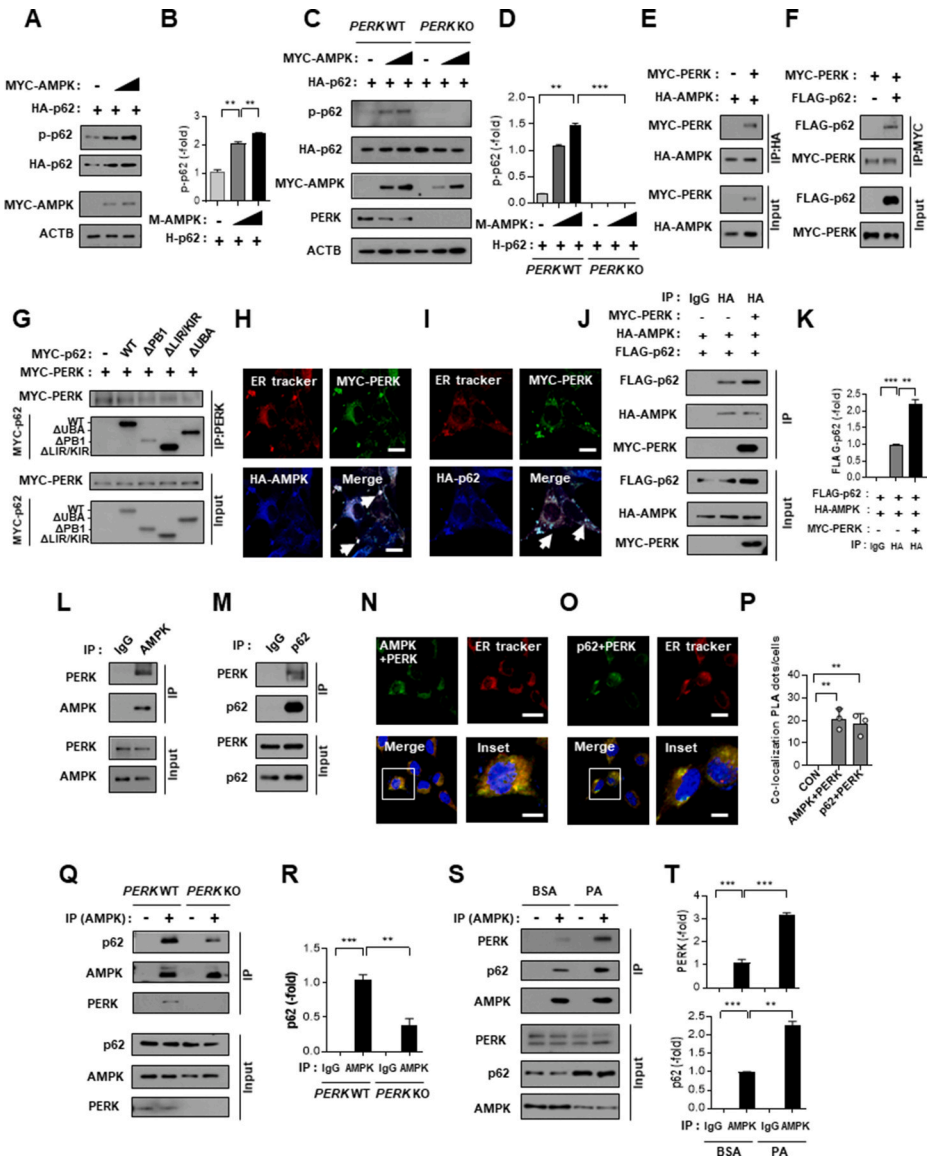

Fig. 3. PERK-mediated phosphorylation of p62 via enhanced interactions between AMPK and p62. (**A**) HEK293 cells transfected with vectors encoding MYC-AMPK and HA-p62 were subjected to immunoblot analysis using antibodies against p-p62, HA-p62, MYC-AMPK, and ACTB (loading control). (**B**) Densitometric analysis of the immunoblot. (**C**) *PERK* WT or *PERK* KO MEFs were transfected with vectors encoding HA-p62 together with those expressing of MYC-AMPK, and subjected to immunoblot analysis. (**D**) Densitometric analysis of the immunoblot. (**E**) Lysates from HEK293 cells transfected with MYC-PERK and HA-AMPK vectors were subjected to immunoprecipitation (IP) with antibodies against HA, and the resulting IPs and whole cell lysates (WCLs) were subjected to immunoblot analysis. (**F**) Lysates from HEK293 cells transfected with vectors encoding MYC-PERK and FLAG-p62 were subjected to IP with antibodies against MYC, and subjected to immunoblot. (**G**) Lysates from HEK293 cells transfected with deletion constructs of MYC-p62 were subjected to IP with antibodies specific for PERK, and were subjected to immunoblot analysis. Representative confocal microscopy images of Hepa1c1c7 cells transfected with vectors encoding MYC-PERK and either HA-AMPK (**H**) or HA-p62 (**I**), showing their co-localization via ER Tracker Red staining. Scale bars: 10 μm. (**J**) Lysates from HEK293 cells transfected with HA-AMPK, FLAG-p62, and MYC-PERK were subjected to IP with antibodies to HA, and were subjected to immunoblot analysis. (**K**) Densitometric analysis of the immunoblot. Lysates from Hepa1c1c7 cells were subjected to IP using antibodies against AMPK (**L**) or p62 (**M**), and were subjected to immunoblot analysis. Representative confocal microscopy images of the PLA (proximity-ligation assay) using PERK and either AMPK (**N**) or p62 (**O**), showing their co-localization via ER Tracker Red staining. Scale bars: 10 μm. (**P**) Quantitative analysis of the percentage of PLA dots that co-localized with the ER tracker. (**Q**) Lysates from *PERK* WT or *PERK* KO MEFs were subjected to IP with antibodies against AMPK, and were subjected to immunoblot analysis. (**R**) Densitometric analysis of the immunoblot. (**S**) Lysates from Hepa1c1c7 cells treated with PA (500 μM) for 18 h were subjected to IP using antibodies against AMPK, and were subjected to immunoblot analysis. (**T**) Densitometric analysis of the immunoblots. Data are presented as the means ± SDs from 3 independent experiments. $^{**}p < 0.01$ and $^{***}p < 0.001$. See also Fig. S3. (For interpretation of the references to color in this figure legend, the reader is referred to the Web version of this article.)

degradation, we treated si*PERK*-mediated knockdown Hepa1c1c7 cells with PA. Our results also showed that autophagic KEAP1 degradation was blocked in PA-treated *PERK* knockdown Hepa1c1c7 cells, followed by downregulation of LC3B-II (Fig. S4A–S4D).

To investigate whether PERK mediates autophagy activation in response to lipotoxicity, we treated *PERK* WT or *PERK* KO MEFs with PA and then evaluated the co-localization of LC3B and LysoTracker. A partial decrease in autolysosome formation was observed in *PERK* KO MEFs under lipotoxic stress (Fig. 4E–F).

To determine whether PERK-induced autophagy activation leads to KEAP1 degradation in response to lipotoxicity, we treated *PERK* WT or *PERK* KO MEFs with PA and bafilomycin A1 (BafA1), most well known as an autophagy inhibitor. We showed that the autophagic degradation of KEAP1 was blocked in BafA1-treated *PERK* KO MEFs. Additionally, we showed that the LC3B-II levels were further increased in BafA1-treated *PERK* WT MEFs compared with those in *PERK* KO MEFs (Fig. 4G–H). Moreover, we examined whether PERK is required for the promotion of autophagic flux under lipotoxic stress. We transfected *PERK* WT or *PERK* KO MEFs with a GFP-RFP-LC3B expression vector and treated them with PA. Our results showed that autophagic flux was increased via detecting the increase levels of red fluorescent protein (RFP)-LC3 puncta and yellow fluorescent protein (YFP)-LC3 puncta in PA-treated *PERK* WT MEFs, but that is decreased in PA-treated *PERK* KO MEFs (Fig. 4I–J).

Next, we examined the effect of *PERK* siRNA transfection in green fluorescent protein (GFP)-conjugated LC3B (GFP-LC3B)-expressing HeLa (GFP-LC3B HeLa) cells under subsequent treatment with PA. Our data showed a significant reduction in the levels of GFP-LC3B-II and LC3B-II in *PERK* knockdown GFP-LC3B-HeLa cells, which resulted in the inhibition of KEAP1 degradation (Fig. 4K–M). We also observed that the number of GFP-LC3B puncta was decreased in si*PERK*-mediated knockdown GFP-LC3B HeLa cells under lipotoxicity (Fig. 4N–O).

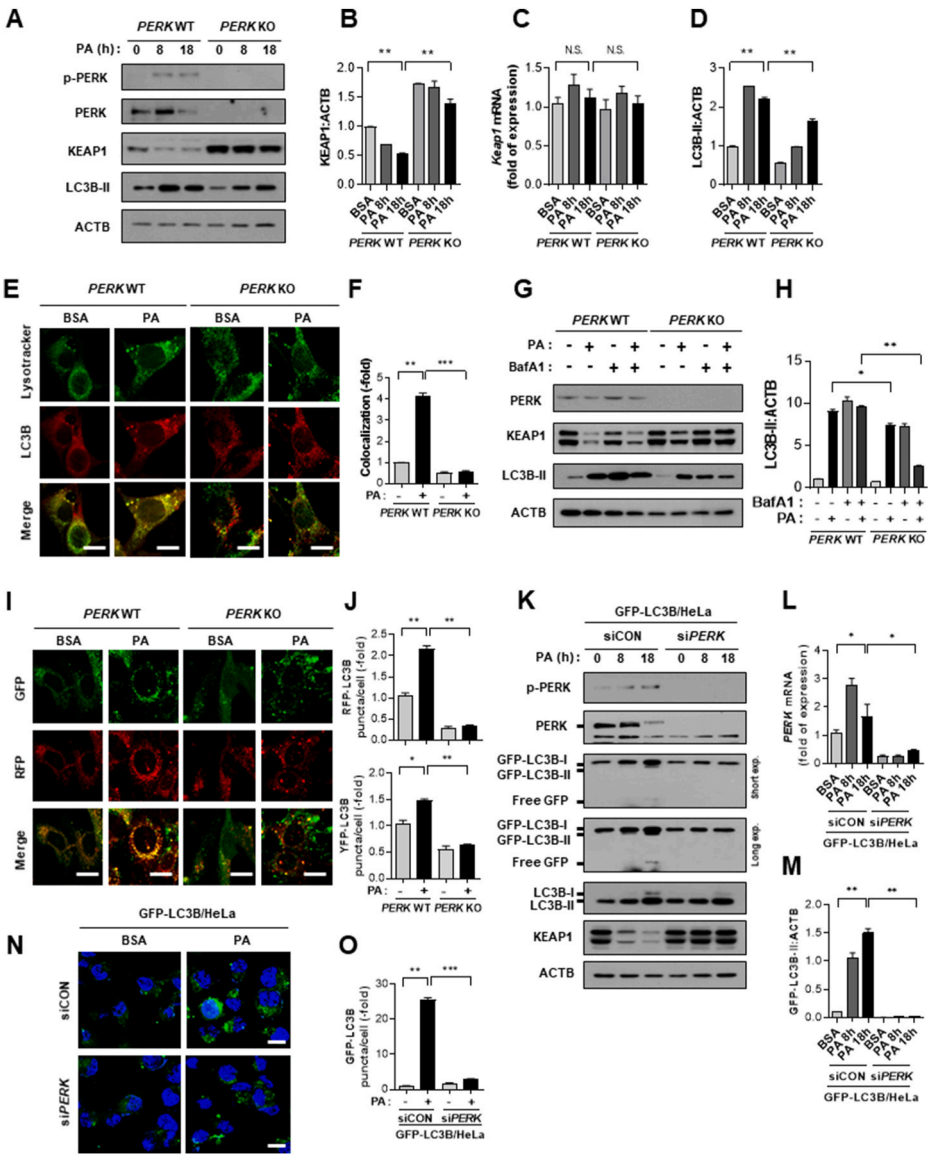

Fig. 4. PERK induces autophagy activation in response to lipotoxicity. (**A**) *PERK* wild-type (WT) or *PERK* knockout (KO) mouse embryonic fibroblasts (MEFs) were incubated with palmitic acid (PA) (500 μM) for the indicated durations. Immunoblot analysis using antibodies against p-PERK, PERK, KEAP1, LC3B, and ACTB (loading control). (**B, D**) Densitometric analysis of the immunoblots. (**C**) qRT-PCR analysis of *Keap1* mRNA. (**E**) Co-localization of LysoTracker and LC3B in *PERK* WT or *PERK* KO MEFs treated with PA (500 μM) as evaluated by confocal microscopy analysis. Representative images are shown. Scale bar: 10 μm. (**F**) Quantitative analysis of the co-localization observed in (**E**). (**G**) *PERK* WT or *PERK* KO MEFs were treated with PA (500 μM) and BafA1 (10 nM) and subjected to immunoblot analysis using antibodies against PERK, KEAP1, LC3B, and ACTB (loading control). (**H**) Densitometric analysis of the LC3B-II immunoblot. (**I**) *PERK* WT or *PERK* KO MEFs transfected with mRFP-GFP-LC3B plasmid were treated with PA. Scale bar: 10 μm. (**J**) Quantitative analysis of red fluorescent protein (RFP)-LC3B and yellow fluorescent protein (YFP)-LC3B. (**K**) GFP-LC3B HeLa cells transfected with control siRNA (20 nM) or *PERK* siRNA (20 nM) and treated with PA for the indicated durations. Immunoblot analysis using antibodies against p-PERK, PERK, GFP, LC3B, KEAP1, and ACTB (loading control). (**L**) qRT-PCR analysis of *PERK* mRNA. (**M**) Densitometric analysis of the GFP-LC3B-II immunoblot. (**N**) GFP-LC3B fluorescence analysis of puncta via confocal microscopy in GFP-LC3B HeLa cells transfected and treated as described in (**K**). Representative single optical sections and merged images are shown. Scale bar: 10 μm. (**O**) Quantitative analysis of GFP-LC3B puncta/cells. Graphical and statistical analyses were performed using GraphPad Prism 9 software. Bar graphs were drawn using the mean values of the results per sample but the statistical significances were derived from raw data. Data are presented as means ± SD from 3 independent experiments. $^{*}p < 0.05$, $^{**}p < 0.01$, $^{***}p < 0.001$, and N.S., not significant. See also Fig. S4. (For interpretation of the references to color in this figure legend, the reader is referred to the Web version of this article.)

Collectively, these findings indicate that PERK can activate autophagy, and subsequently induce autophagic KEAP1 degradation in response to lipotoxicity.

3.5. *PERK directly mediates ULK1 phosphorylation at S317 and induces autophagic KEAP1 degradation*

Recent studies have reported that the AMPK-ULK1 axis induces autophagy activation under nutrient starvation, which is accelerated by the phosphorylation of ULK1 at S317 [46,47]. In addition, our previous study showed that p62-mediated phosphorylation of ULK1 induced autophagy, thereby causing autophagic KEAP1 degradation in response to lipotoxicity [29]. Based on these results, to verify whether PERK mediates ULK1 phosphorylation-induced autophagic KEAP1 degradation, we treated *PERK* WT or *PERK* KO MEFs and *PERK* knockdown Hepa1c1c7 cells with PA. Interestingly, we observed the marked inhibition of ULK1 phosphorylation at the S317 site and KEAP1 degradation in *PERK* KO MEFs (Fig. 5A–C) and also in *PERK* knockdown Hepa1c1c7 cells (Fig. S5A–S5C) in response to PA.

Furthermore, to verify whether PERK mediates ULK1 phosphorylation-induced autophagic KEAP1 degradation, we transfected *PERK* WT or *PERK* KO MEFs with FLAG-ULK1 and HA-KEAP1 expression vectors (Fig. 5D) and also *PERK* knockdown Hepa1c1c7 cells with the vectors (Fig. S5D). We found that the ectopic expression of phosphorylated ULK1 was utterly blocked in both *PERK* KO MEFs (Fig. 5D–E) and *PERK* knockdown Hepa1c1c7 cells (Fig. S5D–S5E). We further observed that ULK1-mediated autophagic KEAP1 degradation is blocked in *PERK* KO MEFs (Fig. 5D-F) and *PERK* knockdown Hepa1c1c7 cells (Figs. S5D and S5F).

To further confirm whether PERK induces ULK1 phosphorylation, followed by autophagy activation, we treated Hepa1c1c7 cells with a PERK inhibitor (GSK2656157) [44,45] under lipotoxic conditions. We found that PERK-mediated ULK1 phosphorylation-induced autophagic KEAP1 degradation was significantly inhibited, followed by a decrease in LC3B-II levels in *PERK*-inactivated cells (Fig. S5G–S5K). Taken together, these results demonstrate that PERK activates autophagy through ULK1 phosphorylation, followed by autophagic KEAP1 degradation in response to lipotoxicity.

We also examined whether PERK could directly phosphorylate ULK1. We first investigated the results of the *in vitro* GST pull-down assay, which provided evidence of the direct binding of ULK1 to PERK (Fig. 5G). To demonstrate that S317 is a direct substrate of PERK, we

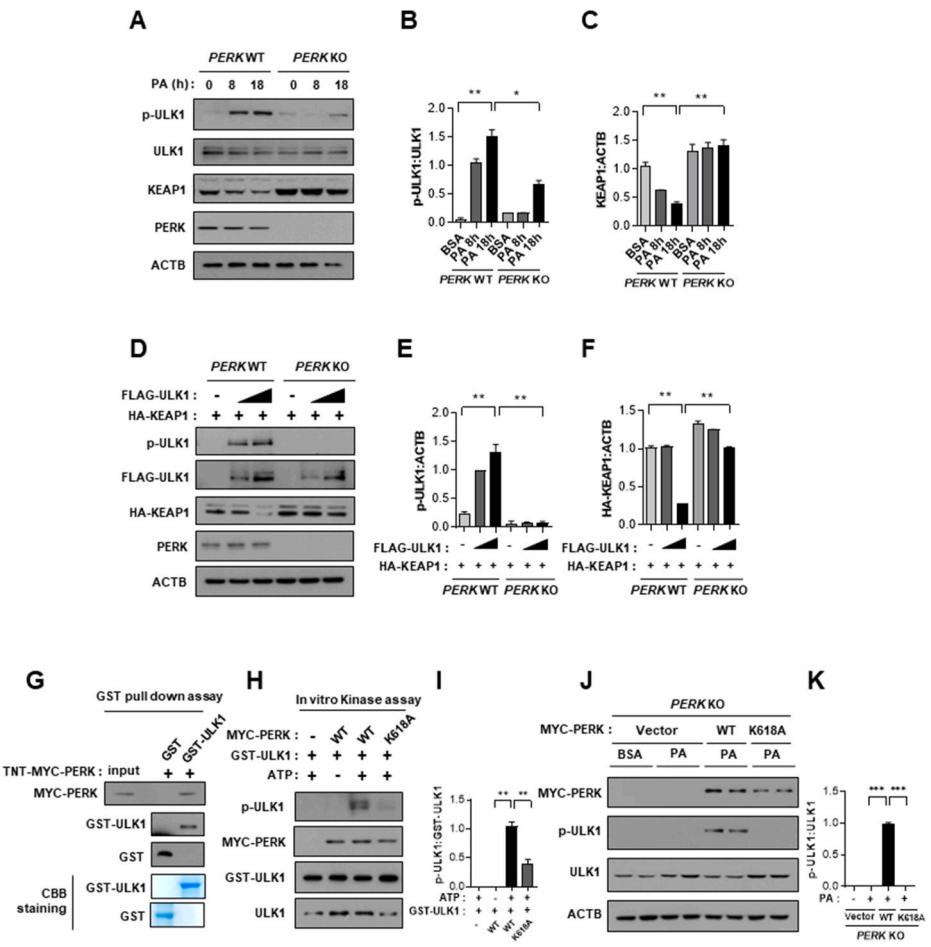

Fig. 5. PERK directly phosphorylates ULK1 at S317 and induces autophagic KEAP1 degradation. (**A**) *PERK* wild-type (WT) or *PERK* knockout (KO) mouse embryonic fibroblasts (MEFs) were treated with palmitic acid (PA) (500 μM) for the indicated durations. Immunoblot analysis with antibodies against p-ULK1, ULK1, KEAP1, PERK, and ACTB (loading control). (**B–C**) Densitometric analysis of the immunoblots. (**D**) *PERK* WT or *PERK* KO MEFs were transfected with vectors encoding FLAG-ULK1 and HA-KEAP1, and subjected to immunoblot analysis using antibodies against p-ULK1, FLAG-ULK1, HA-KEAP1, PERK, and ACTB (loading control). (**E-F**) Densitometric analysis of the immunoblots. (**G**) *In vitro* translated MYC-PERK was subjected to GST pull-down assays using affinity-purified GST or GST-ULK1. The proteins bound to GST-ULK1 were analyzed via immunoblotting using an anti-MYC antibody. The acrylamide gel stained with Coomassie Brilliant Blue (CBB) contained GST and GST-ULK1 used in the pull-down assay. (**H**) *In vitro* kinase assay for ULK1 phosphorylation at the S317 site. GST-ULK1 was used as substrate for MYC-PERK WT or K618A (kinase dead mutant) immunoprecipitated from HEK293 cells. Western blotting analysis was performed using S317 phospho-specific antibodies, as well as MYC, GST, and ULK1 antibodies. (**I**) Densitometric analysis of the immunoblot. (**J**) *PERK* KO MEFs were transfected with MYC-PERK WT or MYC-PERK K618A, and then treated with PA (500 μM) for 18 h. The cells were subjected to immunoblot analysis against MYC-PERK, p-ULK1, ULK1, and ACTB (loading control). (**K**) Densitometric analysis of the immunoblot. Graphical and statistical analyses were performed using GraphPad Prism 9 software. Bar graphs were drawn using the mean values of the results per sample but the statistical significances were derived from raw data. Data are presented as means ± SD from 3 independent experiments. $^{*}p < 0.05$, $^{**}p < 0.01$, and $^{***}p < 0.001$. See also Fig. S5. (For interpretation of the references to color in this figure legend, the reader is referred to the Web version of this article.)

performed an *in vitro* kinase assay using purified GST-tagged ULK1 and immunoprecipitated it with lysates from MYC-PERK WT and MYC-PERK KD (K618A) cells. We expressed MYC-PERK in HEK293 cells and subjected the same to immunoprecipitation using an anti-MYC antibody. The recombinant GST-ULK1 protein was incubated with the PERK immune complex in the presence of ATP. As expected, the PERK WT-complex cells phosphorylate ULK1 at S317, but not in the K618A mutant (Fig. 5H–I). Next, to further demonstrate that PERK induces ULK1 phosphorylation in response to lipotoxicity, we transfected *PERK* KO MEFs with the MYC-PERK WT and MYC-PERK KD expression vectors, then treated the cells with PA. We observed that the MYC-PERK WT-mediated phosphorylation of ULK1 at S317 was significantly inhibited in MYC-PERK KD-expressing cells under lipotoxic conditions (Fig. 5J–K). Collectively, our findings demonstrate that PERK serves as a direct protein kinase of ULK1 for phosphorylation at S317, and thereby activates autophagy in response to lipotoxicity.

3.6. *PERK facilitates the AMPK-ULK1 interaction, inducing ULK1 phosphorylation*

It is well known that AMPK positively regulates ULK1-mediated autophagy [46,47]. Consistently, we showed that AMPK directly interacted with ULK1 through a GST pull-down assay (Fig. S6A). Next, we confirmed that GST-ULK1 was significantly phosphorylated at S317 by AMPK using an *in vitro* kinase assay (Fig. S6B).

To further determine whether the phosphorylation of ULK1 at S317 requires AMPK, we transfected HEK293 cells with MYC-AMPK and HA-ULK1 expression vectors. Based on these observations, we showed that ectopic expression of AMPK significantly increased the phosphorylation of ULK1 at S317 (Fig. 6A–B). Furthermore, we observed a clear inhibition of ULK1 phosphorylation in both *PERK* KO MEFs (Fig. 6C–D) and *PERK* knockdown Hepa1c1c7 cells (Fig. S6C–S6D). These data confirmed that PERK is required for the phosphorylation of ULK1 in an AMPK-dependent manner.

To verify how PERK induces AMPK-mediated ULK1 phosphorylation, we transfected HEK293 cells with MYC-PERK and HA-ULK1 expression vectors and subjected the cell lysates to IP analysis. We found that MYC-PERK interacted with HA-ULK1 (Fig. 6E) even in the absence of a specific binding domain (Fig. 6F, Fig. S6E) and that MYC-PERK and HA-ULK1 were co-localized in the ER (Fig. 6G). To explore whether PERK is involved in the interaction between ULK1 and AMPK, we transfected HEK293 cells with HA-ULK1 and FLAG-AMPK expression vectors together with MYC-PERK and subjected the cell lysates to co-IP analysis. The results showed that PERK facilitated the interaction between ULK1 and AMPK (Fig. 6H–I).

We further observed that endogenous PERK bound to ULK1 in Hepa1c1c7 cells (Fig. 6J). We also investigated the interaction of two proteins (endogenous PERK and ULK1) on the ER following stimulation,

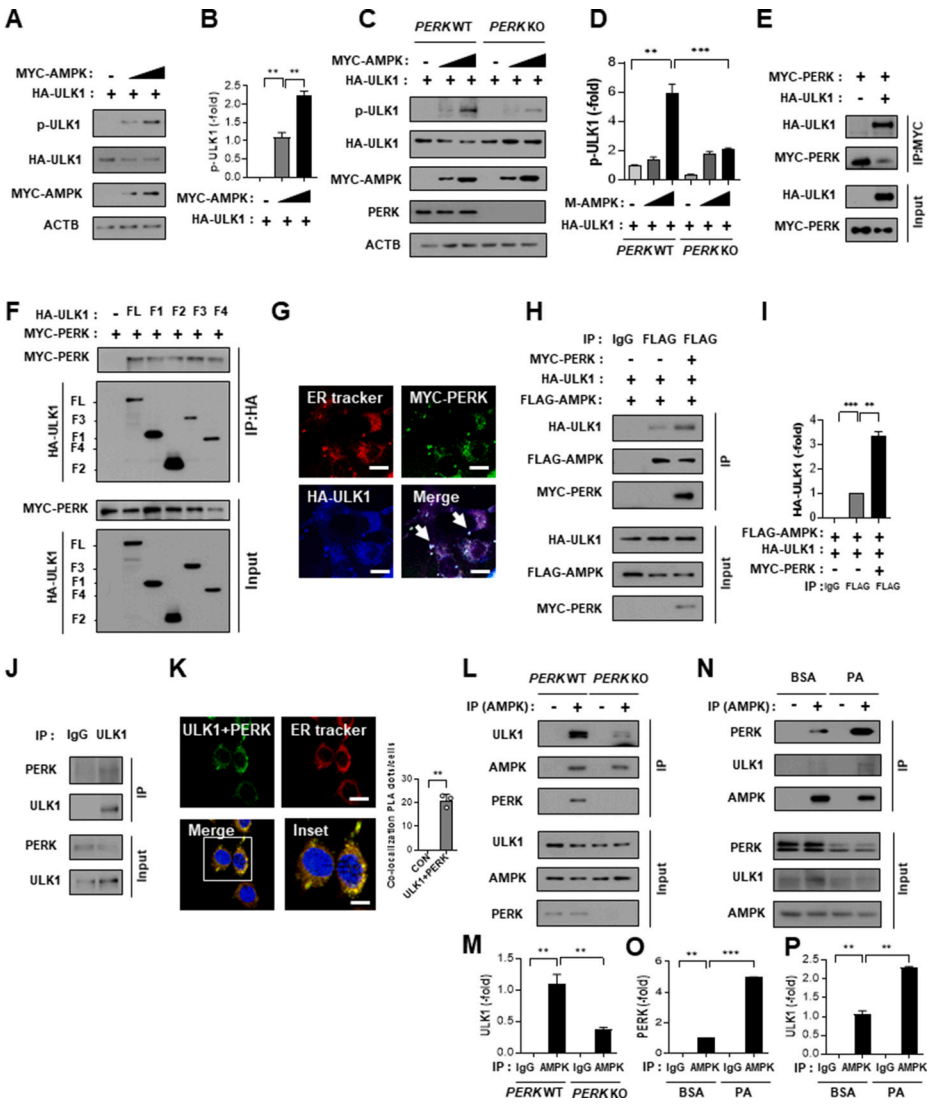

Fig. 6. PERK facilitates the binding of the AMPK-ULK1 complex, inducing ULK1 phosphorylation. (**A**) HEK293 cells transfected with vectors encoding MYC-AMPK and HA-ULK1 were subjected to immunoblot analysis. (**B**) Densitometric analysis of the immunoblot. (**C**) *PERK* WT or *PERK* KO MEFs were transfected with vectors encoding HA-ULK1 together with those expressing of MYC-AMPK, and subjected to immunoblot analysis. (**D**) Densitometric analysis of the immunoblot. (**E**) Lysates of HEK293 cells transfected with MYC-PERK and HA-ULK1 vectors were subjected to IP using antibodies against MYC, then subjected to immunoblot analysis. (**F**) Lysates of HEK293 cells transfected with deletion constructs of HA-ULK1 vectors were subjected to IP using antibodies specific for HA, then the IPs and WCLs were subjected to immunoblot analysis. (**G**) Representative confocal microscopy images of the Hepa1c1c7 cells transfected with vectors encoding MYC-PERK and HA-ULK1, showing their co-localization via ER Tracker Red staining. Scale bars: 10 μm. (**H**) Lysates of HEK293 cells transfected with HA-ULK1, FLAG-AMPK, and MYC-PERK vectors were subjected to IP using antibodies against FLAG, then subjected to immunoblot analysis. (**I**) Densitometric analysis of the immunoblot. (**J**) Lysates of Hepa1c1c7 cells were subjected to IP using antibodies against ULK1, then subjected to immunoblot analysis. (**K**) Representative confocal microscopy images of the PLA (proximity-ligation assay) using PERK and ULK1, showing their co-localization via ER Tracker Red staining. Scale bars: 10 μm. Quantification of the percentage of PLA dots that co-localized with the ER tracker. (**L**) Lysates of *PERK* WT or *PERK* KO MEFs were subjected to IP using antibodies against AMPK, then the IPs and WCLs were subjected to immunoblot analysis. (**M**) Densitometric analysis of the immunoblot. (**N**) Lysates of Hepa1c1c7 cells treated with PA (500 μM) for 18 h were subjected to IP using antibodies against AMPK, then subjected to immunoblot analysis. (**O–P**) Densitometric analysis of the immunoblots. Graphical and statistical analyses were performed using GraphPad Prism 9 software. Bar graphs were drawn using the mean values of the results per sample but the statistical significances were derived from the raw data. Data are presented as the means ± SDs from 3 independent experiments. $^{**}p < 0.01$ and $^{***}p < 0.001$. See also Fig. S6. (For interpretation of the references to color in this figure legend, the reader is referred to the Web version of this article.)

using an *in situ* proximity-ligation assay (PLA) (Fig. 6K). To evaluate the relationship between PERK and the ULK1-AMPK complex, we examined their interactions in *PERK* WT or *PERK* KO MEFs. We found that the binding of ULK1-AMPK was dramatically attenuated in *PERK* KO MEFs (Fig. 6L–M). We further investigated whether the endogenous PERK-p62-AMPK complex was strongly bound in Hepa1c1c7 cells under lipotoxic conditions (Fig. 6N–P). Taken together, we have shown that PERK plays an essential role in facilitating the interaction between ULK1 and AMPK, followed by the induction of AMPK-mediated ULK1 phosphorylation.

3.7. Reinforcement of PERK protects cells against lipotoxicity by activation of the p62-ULK1 axis-induced noncanonical KEAP1-Nrf2 pathway in PERK-deficient cells

To verify whether PERK plays a cytoprotective role against lipotoxicity, we transfected *PERK* KO MEFs with MYC-PERK WT vector and treated them with PA. The results showed that the overexpression of PERK induced the phosphorylation of both p62 and ULK1, which was followed by autophagic KEAP1 degradation and Nrf2 activation in *PERK* KO MEFs under lipotoxic conditions (Fig. 7A–I). Accordingly, PERK rescued PA-induced cell death caused by *PERK* ablation in response to lipotoxicity, as indicated by the decreased levels of C.CASP3 and C.PARP (Fig. 7A, Fig. S7), via activation of the p62-ULK1 axis-mediated non-canonical KEAP1-Nrf2 pathway (Fig. 7A–I). From these results, we conclude that PERK protects cells against lipotoxicity (Fig. 7J–L) and eliminates ROS (Fig. 7M-N) via activation of our suggested pathway.

Taken together, our results demonstrate that the PERK-mediated p62-ULK1 axis-induced noncanonical KEAP1-Nrf2 pathway plays a crucial cytoprotective role against lipotoxicity.

3.8. ER stress-dependent activation of the noncanonical KEAP1-Nrf2 pathway protects the mouse liver against physiological lipotoxicity

Both hepatic ER stress and SFA accumulation are high in patients with NASH [33,48]. To induce physiological lipotoxic stress, mice were fasted overnight, and then refed with a high-carbohydrate, fat-free diet (HCD) [13,29]. In our previous studies, we demonstrated a marked

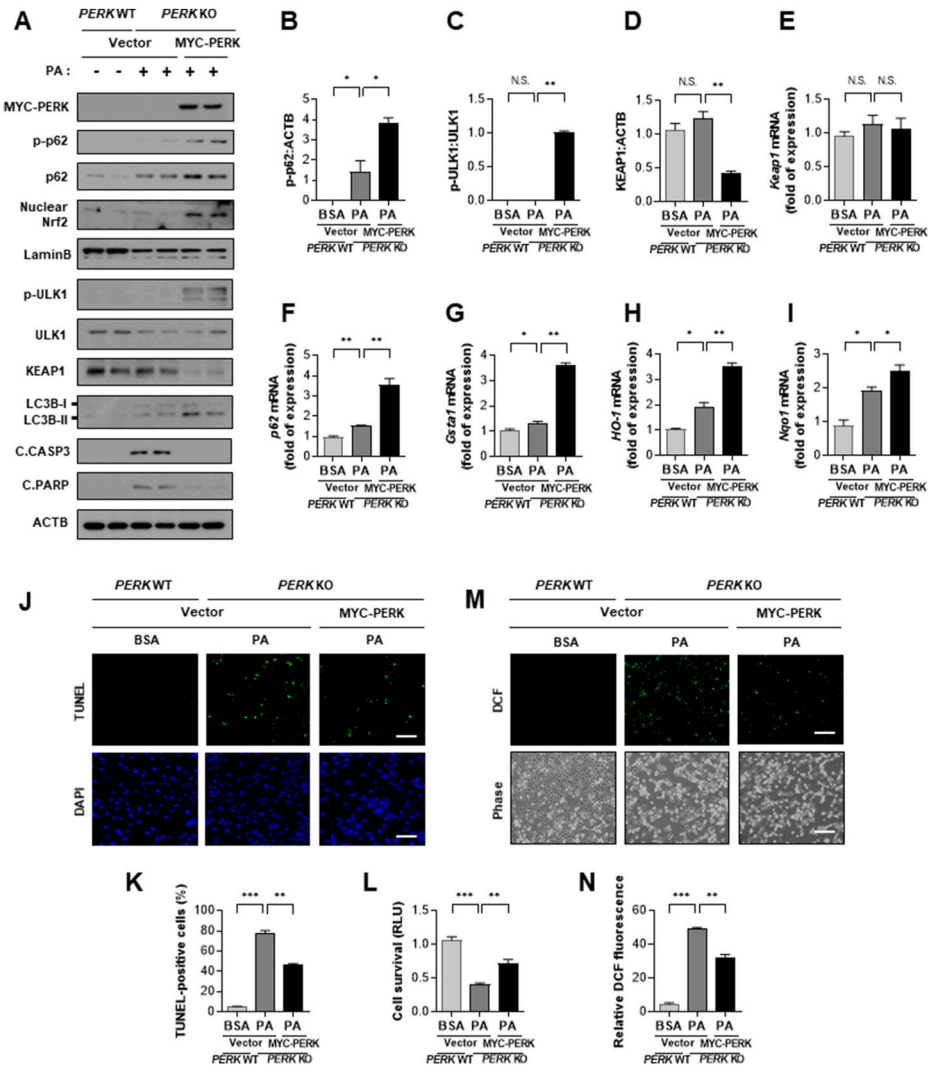

Fig. 7. Reintroduction of PERK in *PERK*-deficient cells attenuates palmitic acid (PA)-induced cell death via activation of the p62-ULK1 axis-mediated noncanonical KEAP1-Nrf2 pathway. (**A**) *PERK* knockout (KO) mouse embryonic fibroblasts (MEFs) were transfected with vector encoding MYC-PERK and treated with PA (500 μM) for 18 h, then subjected to immunoblot analysis for MYC-PERK, p-p62, p62, nuclear Nrf2, LaminB (nucler protein marker), p-ULK1, ULK1, KEAP1, LC3B, cleaved caspase3 (C.CASP3), cleaved PARP (C.PARP), and ACTB (loading control). (**B-D**) Densitometric analysis of the immunoblots. qRT-PCR analysis of the relative mRNA expression of *Keap1* (**E**), *p62* (**F**), *Gsta1* (**G**), *HO-1* (**H**), and *Nqo1* (**I**). (**J**) Terminal deoxynucleotidyl transferase-mediated dUTP nick-end labeling (TUNEL) analysis of the cells treated as described in (**A**). Scale bar: 100 μm. (**K**) Quantification of TUNEL-positive cells. (**L**) Cell viability of the cells treated as in (**A**) as estimated using a Cell Titer-Glo assay kit. (**M**) Reactive oxygen species (ROS) levels were detected using CM-H2DCFH-DA. Representative images are shown. Scale bar: 100 μm. (**N**) Quantitative analysis of the relative levels of DCF fluorescence. Graphical and statistical analyses were performed using GraphPad Prism 9 software. Bar graphs were drawn using the mean values of the results per sample but the statistical significances were derived from raw data. Data are presented as means ± SD from 3 independent experiments. $^{*}p < 0.05$, $^{**}p < 0.01$, $^{***}p < 0.001$, and N.S., not significant. See also Fig. S7. (For interpretation of the references to color in this figure legend, the reader is referred to the Web version of this article.)

increase of PA levels in the mouse liver after refeeding with HCD [29]. Furthermore, hepatic ER stress and the p62-mediated noncanonical KEAP1-Nrf2 pathway are also induced in this physiological setting [13,28,29].

To further investigate whether PA-induced ER stress can activate the p62-dependent noncanonical KEAP1-Nrf2 pathway under physiological lipotoxicity, we injected mice with PBA, which was followed by refeeding with HCD. We found that the activation of the p62-mediated noncanonical KEAP1-Nrf2 pathway was dependent on ER stress in mouse livers (Fig. 8A–G). In addition, we found that ER stress was upregulated during physiological lipotoxicity, which was markedly inhibited in PBA-treated mice, as indicated by the increase in the expression of the Grp78 protein and ER stress target genes (including *Grp78*, *Trb3,* and *Atf4)* (Fig. 8A, 8J-M). Consistent with our *in vitro* findings, we observed that the phosphorylation of PERK was significantly increased in the HCD refed mice and was attenuated in ER stress-inhibited mice (Fig. 8A, 8H–I), whereas the phosphorylation levels of other UPR sensors (IRE1α and cleaved ATF6) were slightly downregulated in ER stress-inhibited mice under physiological lipotoxic conditions (Fig. S8). Furthermore, the results showed that oxidative liver damage was decreased to a greater extent in PBA-treated mice than in untreated mice, as indicated by hematoxylin and eosin (H&E) staining patterns (Fig. 8N), serum alanine aminotransferase (ALT) levels, and findings from the TUNEL assay (Fig. 8O–P). We further evaluated oxidative stress-mediated liver injury was ameliorated in ER stress-inhibited mice, as assessed by immunohistochemistry (IHC) analysis of the oxidative stress markers 3-nitrotyrosine (3-NT) and 4-hydroxynonenal (4HNE) (Fig. 8Q–S).

Collectively, these results indicate that the activation of the p62-mediated noncanonical KEAP1-Nrf2 pathway is dependent on ER stress under lipotoxic conditions in the mouse liver, and PERK may be involved in the activation of this pathway.

3.9. PERK plays a hepatoprotective role against physiological lipotoxicity by activating the p62-ULK1 axis-mediated noncanonical KEAP1-Nrf2 pathway in the mouse liver

To determine whether PERK plays a hepatoprotective role by activating the p62-ULK1 axis-mediated noncanonical KEAP1-Nrf2 pathway under physiological lipotoxic stress in mice, we administered tail vein injections of *PERK* siRNA in B6 mice and subjected the mice to refeeding with HCD [13,29] (Fig. 9). We observed that p62 phosphorylation at S351 and the ULK1 (S317)-mediated autophagic KEAP1 degradation were drastically inhibited in *PERK*-depleted mice, which further inhibited Nrf2 activation under physiological lipotoxic conditions (Fig. 9A–I).

To determine the physiological relevance of this pathway in lipotoxicity, we examined IP analysis using mouse liver lysates. Consistent with the *in vitro* findings, the p62-AMPK-ULK1 complex strongly interacted in response to physiological lipotoxicity, and these interactions

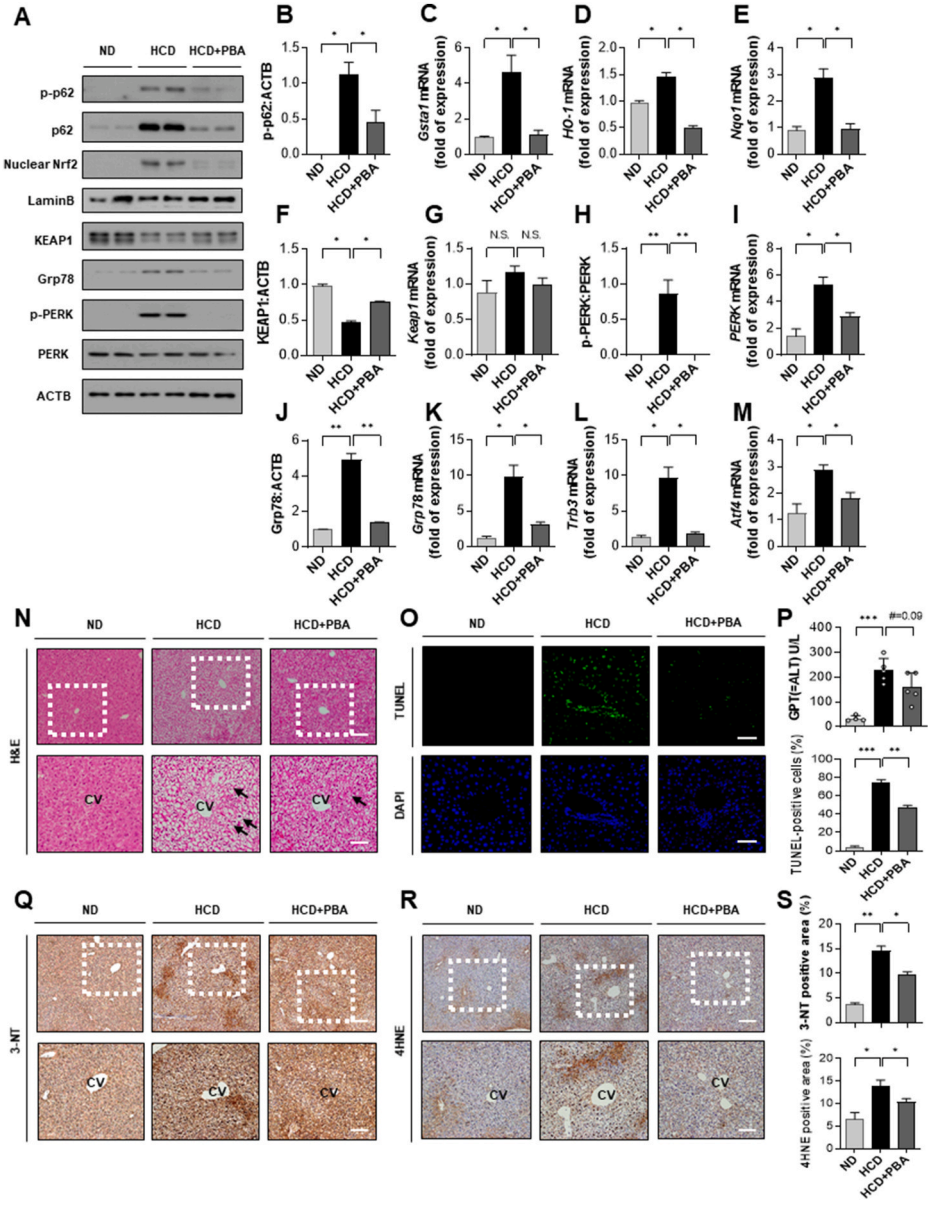

Fig. 8. Activation of the p62-mediated noncanonical KEAP1-Nrf2 pathway is dependent on endoplasmic reticulum (ER) stress and protects the mouse liver against physiological lipotoxicity. Mice were maintained in a non-fasted state and fed normal diet (ND) or overnight fasted stated and then refed a high-carbohydrate, fat-free diet (HCD) with the vehicle or 4-phenylbutyric acid (4-PBA; 20 mg/kg). (**A**) Immunoblot analysis of the liver tissues for p-p62, p62, nuclear Nrf2, LaminB (nucler protein marker), KEAP1, Grp78, p-PERK, PERK, and ACTB (loading control). (**B, F, H, J**) Densitometric analysis of the immunoblots. qRT-PCR analysis of *Gsta1* (**C**), *HO-1* (**D**), *Nqo1* (**E**), *Keap1* (**G**), *PERK* (**I**), *Grp78* (**K**), *Trb3* (**L**), and *Atf4* (**M**) mRNA. (**N**) Liver tissue sections from the mice were stained using hematoxylin and eosin (H&E). CV, central vein. Scale bar: 200 μm. The extent of ballooning degeneration (arrows) is indicated on the images. (**O**) Confocal microscopic images of the terminal deoxynucleotidyl transferase-mediated dUTP nick-end labeling (TUNEL) assay performed using mouse liver sections. Scale bar: 100 μm. (**P**) Serum alanine aminotransferase (ALT) levels and quantification of TUNEL-positive cells were measured in the three groups of mice. (**Q-R**) Liver tissue sections from the mice were subjected to immunohistochemistry (IHC) analysis with antibodies against 3-NT or 4-HNE. Scale bar, 100 μm. (**S**) Quantification of 3-NT- and 4-HNE-positive areas in the three groups of mice. Graphical and statistical analyses were performed using GraphPad Prism 9 software. Bar graphs were drawn using the mean values of the results per sample but the statistical significances were derived from raw data. Data are presented relative to the corresponding values for non-fasted mice and represent the means ± standard errors values for 4 to 5 mice per group. $*p < 0.05$, $**p < 0.01$, $***p < 0.001$, $\#p = 0.09$, and N.S., not significant. See also Fig. S8. (For interpretation of the references to color in this figure legend, the reader is referred to the Web version of this article.)

were markedly decreased in PERK-depleted mice (Fig. 9J–M). These findings suggest that PERK plays a crucial role in facilitating the enhanced interaction between p62 and ULK1 *in vivo*. Next, we showed that liver injury was exacerbated in *PERK*-depleted mice under physiological lipotoxic conditions, as determined using serum ALT levels measurement (Fig. 9N), H&E staining (Fig. 9O), and the TUNEL assay (Fig. 9P–Q); this corresponded to elevated the expression levels of ER stress target genes as well (Figs. S9A–S9C). Furthermore, we also showed the levels of oxidative stress markers including 3-NT and 4HNE were increased in the livers of *PERK*-depleted mice as evaluated by IHC analysis (Fig. 9R-U).

Taken together, these results demonstrate that PERK protects the mouse liver against physiological lipotoxicity through activation of the p62-ULK1 axis-mediated noncanonical KEAP1-Nrf2 pathway.

4. Discussion

The global prevalence of NASH is increasing, and NASH is the most common cause of chronic liver diseases, induced by SFA-mediated hepatic lipotoxicity [7]. Excessive SFA production induces ER stress, which is significantly high in the livers of patients with NASH and is associated with impaired autophagy [49,50]. SFA-mediated ER stress sequentially induces ROS accumulation, which can cause oxidative stress-mediated hepatocyte injury by inhibiting mitochondrial respiration and blocking membrane sodium channels [3,4]. Moreover, ROS promotes lipid peroxidation and cytokine production, further contributing to NASH development [51].

Currently, there are no available pharmacological treatments for NASH. Recent studies have focused on the activation of the master transcription factor Nrf2 for the development of therapies for NASH because Nrf2 is known to regulate antioxidant synthesis and ROS-eliminating enzyme expression [52–54]. Canonical Nrf2 activation is mediated via KEAP1 oxidation by electrophilic compounds [12,55]. However, this canonical pathway exhibits non-specific activity because different cysteine residues in various proteins can be oxidized by canonical Nrf2 activators, which limits their utility [16].

Accordingly, more specific compounds that act through the noncanonical pathway are known to serve as excellent targets for Nrf2 activation. p62 is the most notable substrate of the noncanonical KEAP1-Nrf2 pathway [16]. p62 disrupts the interaction between KEAP1 and

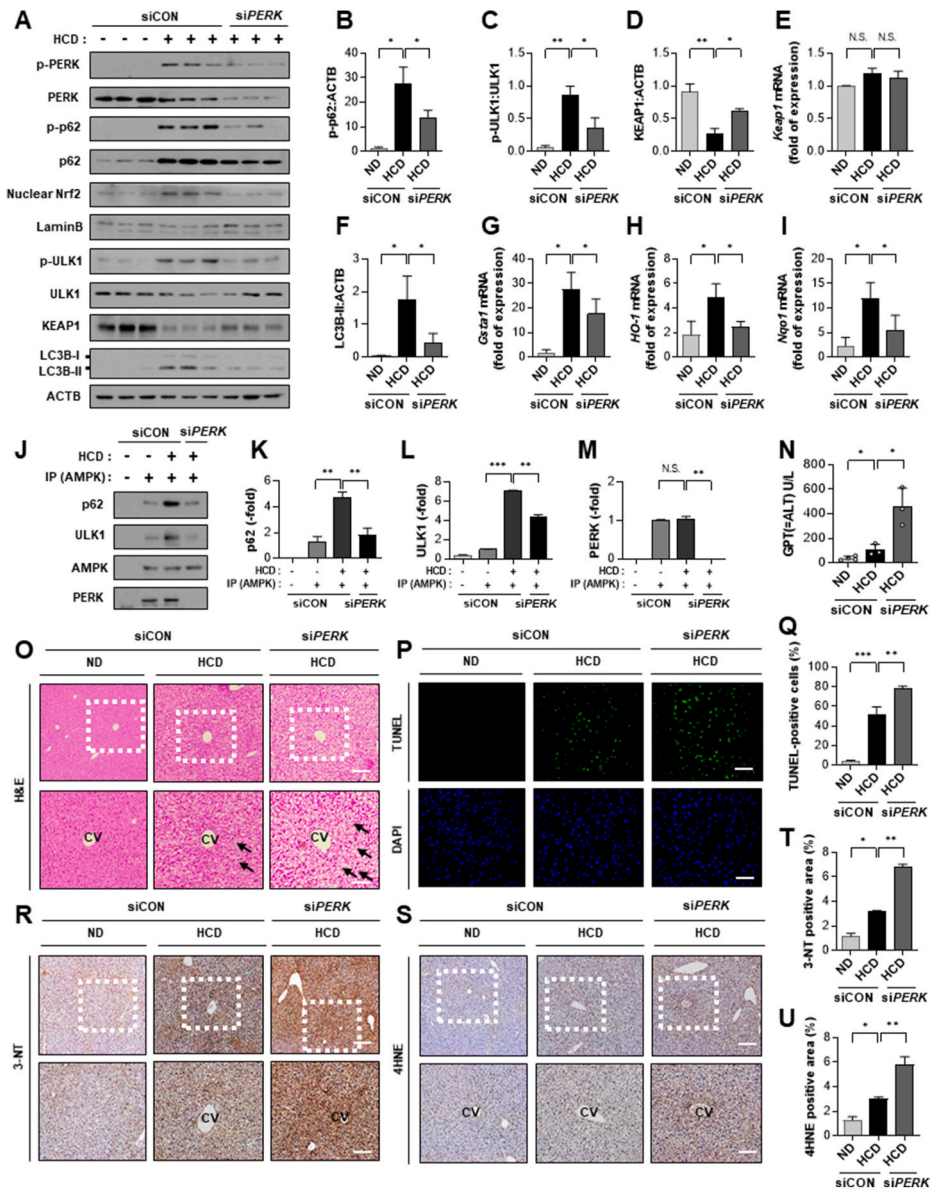

Fig. 9. PERK prevents hepatic lipotoxicity via activation of the p62-ULK1 axis-mediated non-canonical KEAP1-Nrf2 pathway and autophagy in mouse liver. Mice injected with control siRNA (20 nM) or *PERK* siRNA (20 nM) via tail vein were maintained in a non-fasted state and fed normal diet (ND) or were fasted overnight and then refed a high-carbohydrate, fat-free diet (HCD). (**A**) Immunoblot analysis of the liver tissues using antibodies against p-PERK, PERK, p-p62, p62, nuclear Nrf2, LaminB (nucler protein marker), p-ULK1, ULK1, KEAP1, LC3B, and ACTB (loading control). (**B-D, F**) Densitometric analysis of the immunoblots. qRT-PCR analysis of *Keap1* (**E**), *Gsta1* (**G**), *HO-1* (**H**), and *Nqo1* (**I**) mRNA. (**J**) Lysates of the liver tissues were subjected to IP using antibodies against AMPK, then subjected to immunoblot analysis. (**K-M**) Densitometric analysis of the immunoblots. (**N**) Serum alanine aminotransferase (ALT) levels were measured in mice. (**O**) Liver tissue sections were subjected to hematoxylin and eosin (H&E) staining. CV, central vein. Scale bar: 200 μm. The extent of ballooning degeneration (arrows) is indicated on the images. (**P**) Confocal microscopic images of the terminal deoxynucleotidyl transferase-mediated dUTP nick-end labeling (TUNEL) analysis of liver tissue sections from mice. Scale bar: 200 μm. (**Q**) Quantitative analysis of the TUNEL-positive cells. (**R-S**) Liver sections from mice were subjected to immunohistochemistry (IHC) analysis with antibodies against 3-NT or 4-HNE. Scale bar, 100 μm. (**T-U**) Quantification of 3-NT- and 4-HNE-positive areas in the three groups of mice. Graphical and statistical analyses were performed using GraphPad Prism 9 software. Bar graphs were drawn using the mean values of the results per sample, but the statistical significances were derived from raw data. Data are presented relative to the corresponding value for non-fasted mice and represent the mean ± standard error values for 3 to 4 mice per group. $^{*}p < 0.05$, $^{**}p < 0.01$, $^{***}p < 0.001$, and N.S., not significant. See also Fig. S9. (For interpretation of the references to color in this figure legend, the reader is referred to the Web version of this article.)

Nrf2 by competing with KEAP1 for binding to the DLG motif, thereby activating this pathway in the absence of KEAP1 oxidation [13–15]. The accumulation of p62 in hepatocytes is enhanced by impaired autophagy, which is a critical histological feature of NASH [49,56,57].

Previously, we reported that the p62-mediated noncanonical KEAP1-Nrf2 pathway plays a protective role against ER stress induced by tunicamycin [58]. Moreover, p62 facilitates autophagy activation, followed by autophagic KEAP1 degradation and Nrf2 activation, which prevents SFA-induced ROS accumulation [13,26,29]. We further determined the clinical significance of this pathway in the liver of patients with NAFLD [29]. The p62-mediated noncanonical KEAP1-Nrf2 pathway is activated by the phosphorylation of p62 at S351, which enhances the binding of p62 to KEAP1 with the ETGE motif, followed by increased Nrf2 activation [15,59]. To date, several protein kinases have been shown to phosphorylate p62 at S351 [15] in different cellular contexts. These include mammalian targets of rapamycin complex 1 upon exposure to the oxidative stressor sodium arsenite [15,60], transforming growth factor β-activated kinase 1 under basal conditions [61], and protein kinase C delta under curcumin-induced oxidative stress [62]. Moreover, we previously identified that AMPK phosphorylates p62 (S351) via direct interaction [17]. However, the kinase that directly phosphorylates p62 at S351 in response to lipotoxicity remains unknown.

Lipotoxicity is known to be associated with ER stress, which can be ameliorated through the UPR, an adaptive and defensive pathway that restores ER homeostasis and is controlled by the three stress sensors, IRE1, PERK, and ATF6 [36,63]. Here, we found that one of the UPR sensors, PERK, is responsible for the phosphorylation of p62 at S351 because it accelerates the interaction between AMPK and p62, as well as the direct phosphorylation of p62 through kinase activity. We demonstrated that PERK activates the p62-mediated noncanonical KEAP1-Nrf2 pathway and plays a protective role against lipotoxic stress. It is known that PERK phosphorylates Nrf2, leading to its dissociation from KEAP1, which is followed by activation of the antioxidant response under ER stress [64,65]. Furthermore, PERK increases the expression of ATF4, which is an Nrf2-interacting protein [66], thereby playing the role of an antioxidant under ER stress-induced ROS accumulation [67–71].

Autophagy plays a vital role in NASH [50,72]. Because the suppression of autophagic flux is associated with increased ER stress in the livers of patients with NASH [49], an increase of autophagic flux improves NASH [73,74] and hepatic fibrosis [75] in mouse experimental models. Furthermore, it was shown that chemical chaperone 4-PBA, an

ER stress inhibitor, ameliorates lipid accumulation and lipotoxicity in human hepatoma cells by activating autophagy [76]. ULK1 plays a central role in the initiation stage of the autophagy pathway [77]. ULK1 has multiple serine residues, such as S317 and S777, which AMPK can directly phosphorylate under nutritional deprivation and hypoxic conditions. Therefore, the AMPK-ULK1 axis positively regulates autophagy [46,78]. In our previous study, we reported that ULK1 induces autophagic KEAP1 degradation in response to lipotoxicity, thereby activating Nrf2 and attenuating SFA-mediated ROS accumulation [28]. Although we found that the phosphorylation of ULK1 at S317 is upregulated in this context, which can lead to an increase in autophagic flux [28,29], a mediator with direct kinase activity for ULK1 phosphorylation is yet to be identified.

In the present study, we demonstrated for the first time that PERK may serve as a key regulator of autophagy under lipotoxic conditions. We found that PERK increases autophagic flux via its kinase activity and enhancing the binding of AMPK-ULK1 axis, thereby mediates the phosphorylation of ULK1 at S317, which could subsequently induce autophagic KEAP1 degradation and Nrf2 activation under lipotoxic conditions.

Several studies have reported that the PERK-mediated induction of ATF4 can increase the expression levels of autophagy-related genes, which are required for autophagosome formation, thereby leading to autophagy activation under tunicamycin-induced ER stress [69,70,79,80]. Consistently, we observed that PERK-mediated autophagic KEAP1 degradation is partially dependent on ATF4 (data not shown). Furthermore, we found that the p62-ULK1 axis-mediated noncanonical KEAP1-Nrf2 pathway and autophagy could not be activated in *PERK*--depleted mice under physiological lipotoxic conditions, and this was accompanied by the acceleration of severe liver injury indicated by an increase in hepatocellular ballooning, serum ALT levels, and apoptotic cell death. Consistent with our *in vitro* findings, the formation of the augmented p62-AMPK-ULK1 complex was significantly blocked in *PERK*-depleted mice under physiological lipotoxic stress.

Taken together, these results provide novel insights into the mechanisms by which PERK directly activates the p62-ULK1 axis-mediated noncanonical KEAP1-Nrf2 pathway and thus plays a hepatoprotective role under lipotoxic conditions.

5. Conclusion

The UPR is the primary defense mechanism against ER stress [81], but insufficient UPR activation aggravates the susceptibility of liver tissues to ER stress-mediated lipotoxicity [82]. Therefore, our findings suggest the next line of defense against ER stress-mediated lipotoxicity. In addition, we elucidated the molecular mechanism underlying the p62-mediated noncanonical KEAP1-Nrf2 pathway, which may serve as a promising new therapeutic target strategy against lipotoxicity in NASH treatment (Fig. S9D).

Funding

This work was supported by the National Research Foundation of Korea (NRF) grant funded by the Korea government (MSIT) (NRF-2021R1C1C2095694 to D.H. Lee; NRF-2017R1A2B4007400 to S.H. Bae; NRF-2017R1D1A1B03032808 to J.S. Park). This study was also supported by a Faculty Research Grant from the Yonsei University College of Medicine (6-2019-0068 to S.H. Bae). The study was also supported by a grant from the Korea Health Technology R&D Project through the Korea Health Industry Development Institute, funded by the Ministry of Health & Welfare, Republic of Korea (HI17C0913 and HI16C0257 to S. H. Bae).

Author contributions

S.H. Bae conceived the ideas behind the study. D.H. Lee developed the theory and carried out the experiments with support from J.S. Park and Y.S. Lee contributed to animal experiments. All authors discussed the results and contributed to the final manuscript.

Declaration of competing interest

All authors declare no competing interests.

Acknowledgements

We thank S. H. Back for providing the *PERK* MEFs. GFP-LC3B HeLa cells were kindly provided by M.J. Lee. FLAG- and GST-tagged ULK1 cDNAs were kindly provided by J. Kim and S–W Yu. We thank T. Johansen for providing GST-tagged p62 cDNAs. RFP-GFP-tagged LC3B cDNA was kindly provided by S. G. Rhee. We thank M. Komatsu, S.G. Rhee, J. Han, and C. Lee for their encouragement and insightful comments.

Appendix A. Supplementary data

Supplementary data to this article can be found online at https://doi.org/10.1016/j.redox.2022.102235.

References

[1] X.Q. Zhang, C.F. Xu, C.H. Yu, W.X. Chen, Y.M. Li, Role of endoplasmic reticulum stress in the pathogenesis of nonalcoholic fatty liver disease, World J. Gastroenterol. 20 (7) (2014) 1768–1776.
[2] C. Lebeaupin, D. Vallee, Y. Hazari, C. Hetz, E. Chevet, B. Bailly-Maitre, Endoplasmic reticulum stress signalling and the pathogenesis of non-alcoholic fatty liver disease, J. Hepatol. 69 (4) (2018) 927–947.
[3] R.T. Brookheart, C.I. Michel, J.E. Schaffer, As a matter of fat, Cell Metabol. 10 (1) (2009) 9–12.
[4] M. Fuchs, A.J. Sanyal, Lipotoxicity in NASH, J. Hepatol. 56 (1) (2012) 291–293.
[5] A.V. Snezhkina, A.V. Kudryavtseva, O.L. Kardymon, M.V. Savvateeva, N. V. Melnikova, G.S. Krasnov, et al., ROS generation and antioxidant defense systems in normal and malignant cells, Oxid. Med. Cell. Longev. 2019 (2019), 6175804.
[6] M. Masarone, V. Rosato, M. Dallio, A.G. Gravina, A. Aglitti, C. Loguercio, et al., Role of oxidative stress in pathophysiology of nonalcoholic fatty liver disease, Oxid. Med. Cell. Longev. 2018 (2018), 9547613.
[7] Z. Chen, R. Tian, Z. She, J. Cai, H. Li, Role of oxidative stress in the pathogenesis of nonalcoholic fatty liver disease, Free Radic. Biol. Med. 152 (2020) 116–141.
[8] T.W. Kensler, N. Wakabayashi, S. Biswal, Cell survival responses to environmental stresses via the Keap1-Nrf2-ARE pathway, Annu. Rev. Pharmacol. Toxicol. 47 (2007) 89–116.
[9] K. Itoh, J. Mimura, M. Yamamoto, Discovery of the negative regulator of Nrf2, Keap1: a historical overview, Antioxidants Redox Signal. 13 (11) (2010) 1665–1678.
[10] K. Taguchi, H. Motohashi, M. Yamamoto, Molecular mechanisms of the Keap1-Nrf2 pathway in stress response and cancer evolution, Gene Cell. 16 (2) (2011) 123–140.
[11] R. Shimozono, Y. Asaoka, Y. Yoshizawa, T. Aoki, H. Noda, M. Yamada, et al., Nrf2 activators attenuate the progression of nonalcoholic steatohepatitis-related fibrosis in a dietary rat model, Mol. Pharmacol. 84 (1) (2013) 62–70.
[12] K. Itoh, N. Wakabayashi, Y. Katoh, T. Ishii, K. Igarashi, J.D. Engel, et al., Keap1 represses nuclear activation of antioxidant responsive elements by Nrf2 through binding to the amino-terminal Neh2 domain, Genes Dev. 13 (1) (1999) 76–86.
[13] S.H. Bae, S.H. Sung, S.Y. Oh, J.M. Lim, S.K. Lee, Y.N. Park, et al., Sestrins activate Nrf2 by promoting p62-dependent autophagic degradation of Keap1 and prevent oxidative liver damage, Cell Metabol. 17 (1) (2013) 73–84.
[14] M. Komatsu, H. Kurokawa, S. Waguri, K. Taguchi, A. Kobayashi, Y. Ichimura, et al., The selective autophagy substrate p62 activates the stress responsive transcription factor Nrf2 through inactivation of Keap1, Nat. Cell Biol. 12 (3) (2010) 213–223.
[15] Y. Ichimura, S. Waguri, Y.S. Sou, S. Kageyama, J. Hasegawa, R. Ishimura, et al., Phosphorylation of p62 activates the Keap1-Nrf2 pathway during selective autophagy, Mol. Cell 51 (5) (2013) 618–631.
[16] C.A. Silva-Islas, P.D. Maldonado, Canonical and non-canonical mechanisms of Nrf2 activation, Pharmacol. Res. 134 (2018) 92–99.
[17] D.H. Lee, D.H. Han, K.T. Nam, J.S. Park, S.H. Kim, M. Lee, et al., Ezetimibe, an NPC1L1 inhibitor, is a potent Nrf2 activator that protects mice from diet-induced nonalcoholic steatohepatitis, Free Radic. Biol. Med. 99 (2016) 520–532.
[18] H. Malhi, R.J. Kaufman, Endoplasmic reticulum stress in liver disease, J. Hepatol. 54 (4) (2011) 795–809.
[19] P. Puri, F. Mirshahi, O. Cheung, R. Natarajan, J.W. Maher, J.M. Kellum, et al., Activation and dysregulation of the unfolded protein response in nonalcoholic fatty liver disease, Gastroenterology 134 (2) (2008) 568–576.
[20] A.D. Lake, P. Novak, R.N. Hardwick, B. Flores-Keown, F. Zhao, W.T. Klimecki, et al., The adaptive endoplasmic reticulum stress response to lipotoxicity in

progressive human nonalcoholic fatty liver disease, Toxicol. Sci. 137 (1) (2014) 26–35.
[21] X. Liu, R.M. Green, Endoplasmic reticulum stress and liver diseases, Liver Res. 3 (1) (2019) 55–64.
[22] Y. Wei, D. Wang, F. Topczewski, M.J. Pagliassotti, Saturated fatty acids induce endoplasmic reticulum stress and apoptosis independently of ceramide in liver cells, Am. J. Physiol. Endocrinol. Metab. 291 (2) (2006) E275–E281.
[23] Y.R. Kim, E.J. Lee, K.O. Shin, M.H. Kim, Y. Pewzner-Jung, Y.M. Lee, et al., Hepatic triglyceride accumulation via endoplasmic reticulum stress-induced SREBP-1 activation is regulated by ceramide synthases, Exp. Mol. Med. 51 (11) (2019) 1–16.
[24] A. Higa, E. Chevet, Redox signaling loops in the unfolded protein response, Cell. Signal. 24 (8) (2012) 1548–1555.
[25] C.J. Adams, M.C. Kopp, N. Larburu, P.R. Nowak, M.M.U. Ali, Structure and molecular mechanism of ER stress signaling by the unfolded protein response signal activator IRE1, Front. Mol. Biosci. 6 (2019) 11.
[26] J.S. Park, D.H. Kang, D.H. Lee, S.H. Bae, Concerted action of p62 and Nrf2 protects cells from palmitic acid-induced lipotoxicity, Biochem. Biophys. Res. Commun. 466 (1) (2015) 131–137.
[27] S.C. Cazanave, J.L. Mott, S.F. Bronk, N.W. Werneburg, C.D. Fingas, X.W. Meng, et al., Death receptor 5 signaling promotes hepatocyte lipoapoptosis, J. Biol. Chem. 286 (45) (2011) 39336–39348.
[28] J.S. Park, D.H. Lee, Y.S. Lee, E. Oh, K.H. Bae, K.J. Oh, et al., Dual roles of ULK1 (unc-51 like autophagy activating kinase 1) in cytoprotection against lipotoxicity, Autophagy 16 (1) (2020) 86–105.
[29] D.H. Lee, J.S. Park, Y.S. Lee, J. Han, D.K. Lee, S.W. Kwon, et al., SQSTM1/p62 activates NFE2L2/NRF2 via ULK1-mediated autophagic KEAP1 degradation and protects mouse liver from lipotoxicity, Autophagy (2020) 1–25.
[30] D.W. Choi, W. Na, M.H. Kabir, E. Yi, S. Kwon, J. Yeom, et al., WIP1, a homeostatic regulator of the DNA damage response, is targeted by HIPK2 for phosphorylation and degradation, Mol. Cell 51 (3) (2013) 374–385.
[31] J.H. Kim, D. Seo, S.J. Kim, D.W. Choi, J.S. Park, J. Ha, et al., The deubiquitinating enzyme USP20 stabilizes ULK1 and promotes autophagy initiation, EMBO Rep. 19 (4) (2018).
[32] A.K. Leamy, R.A. Egnatchik, J.D. Young, Molecular mechanisms and the role of saturated fatty acids in the progression of non-alcoholic fatty liver disease, Prog. Lipid Res. 52 (1) (2013) 165–174.
[33] R.H. Lambertucci, S.M. Hirabara, R. Silveira Ldos, A.C. Levada-Pires, R. Curi, T. C. Pithon-Curi, Palmitate increases superoxide production through mitochondrial electron transport chain and NADPH oxidase activity in skeletal muscle cells, J. Cell. Physiol. 216 (3) (2008) 796–804.
[34] H. Malhi, S.F. Bronk, N.W. Werneburg, G.J. Gores, Free fatty acids induce JNK-dependent hepatocyte lipoapoptosis, J. Biol. Chem. 281 (17) (2006) 12093–12101.
[35] G.V. Richieri, A.M. Kleinfeld, Unbound free fatty acid levels in human serum, J. Lipid Res. 36 (2) (1995) 229–240.
[36] B.M. Gardner, D. Pincus, K. Gotthardt, C.M. Gallagher, P. Walter, Endoplasmic reticulum stress sensing in the unfolded protein response, Cold Spring Harbor Perspect. Biol. 5 (3) (2013), a013169.
[37] A. Malo, B. Kruger, B. Goke, C.H. Kubisch, 4-Phenylbutyric acid reduces endoplasmic reticulum stress, trypsin activation, and acinar cell apoptosis while increasing secretion in rat pancreatic acini, Pancreas 42 (1) (2013) 92–101.
[38] C.S. Achard, D.R. Laybutt, Lipid-induced endoplasmic reticulum stress in liver cells results in two distinct outcomes: adaptation with enhanced insulin signaling or insulin resistance, Endocrinology 153 (5) (2012) 2164–2177.
[39] X. Ma, W. Du, S. Shao, C. Yu, L. Zhou, F. Jing, Vildagliptin can alleviate endoplasmic reticulum stress in the liver induced by a high fat diet, BioMed Res. Int. 2018 (2018), 5045182.
[40] X.Q. Zhang, Y. Pan, C.H. Yu, C.F. Xu, L. Xu, Y.M. Li, et al., PDIA3 knockdown exacerbates free fatty acid-induced hepatocyte steatosis and apoptosis, PLoS One 10 (7) (2015), e0133882.
[41] Y. Kitai, H. Ariyama, N. Kono, D. Oikawa, T. Iwawaki, H. Arai, Membrane lipid saturation activates IRE1alpha without inducing clustering, Gene Cell. 18 (9) (2013) 798–809.
[42] T. Yamamoto, J. Endo, M. Kataoka, T. Matsuhashi, Y. Katsumata, K. Shirakawa, et al., Palmitate induces cardiomyocyte death via inositol requiring enzyme-1 (IRE1)-mediated signaling independent of X-box binding protein 1 (XBP1), Biochem. Biophys. Res. Commun. 526 (1) (2020) 122–127.
[43] L. Deldicque, P.D. Cani, A. Philp, J.M. Raymackers, P.J. Meakin, M.L. Ashford, et al., The unfolded protein response is activated in skeletal muscle by high-fat feeding: potential role in the downregulation of protein synthesis, Am. J. Physiol. Endocrinol. Metab. 299 (5) (2010) E695–E705.
[44] C. Atkins, Q. Liu, E. Minthorn, S.Y. Zhang, D.J. Figueroa, K. Moss, et al., Characterization of a novel PERK kinase inhibitor with antitumor and antiangiogenic activity, Cancer Res. 73 (6) (2013) 1993–2002.
[45] J.M. Axten, S.P. Romeril, A. Shu, J. Ralph, J.R. Medina, Y. Feng, et al., Discovery of GSK2656157: an optimized PERK inhibitor selected for preclinical development, ACS Med. Chem. Lett. 4 (10) (2013) 964–968.
[46] J. Kim, M. Kundu, B. Viollet, K.L. Guan, AMPK and mTOR regulate autophagy through direct phosphorylation of Ulk1, Nat. Cell Biol. 13 (2) (2011) 132–141.
[47] D. Egan, J. Kim, R.J. Shaw, K.L. Guan, The autophagy initiating kinase ULK1 is regulated via opposing phosphorylation by AMPK and mTOR, Autophagy 7 (6) (2011) 643–644.
[48] A. Baiceanu, P. Mesdom, M. Lagouge, F. Foufelle, Endoplasmic reticulum proteostasis in hepatic steatosis, Nat. Rev. Endocrinol. 12 (12) (2016) 710–722.
[49] A. Gonzalez-Rodriguez, R. Mayoral, N. Agra, M.P. Valdecantos, V. Pardo, M. E. Miquilena-Colina, et al., Impaired autophagic flux is associated with increased endoplasmic reticulum stress during the development of NAFLD, Cell Death Dis. 5 (2014), e1179.
[50] M. Amir, M.J. Czaja, Autophagy in nonalcoholic steatohepatitis, Expet Rev. Gastroenterol. Hepatol. 5 (2) (2011) 159–166.
[51] F. Ucar, S. Sezer, S. Erdogan, S. Akyol, F. Armutcu, O. Akyol, The relationship between oxidative stress and nonalcoholic fatty liver disease: its effects on the development of nonalcoholic steatohepatitis, Redox Rep. 18 (4) (2013) 127–133.
[52] D. Xu, M. Xu, S. Jeong, Y. Qian, H. Wu, Q. Xia, et al., The role of Nrf2 in liver disease: novel molecular mechanisms and therapeutic approaches, Front. Pharmacol. 9 (2018) 1428.
[53] S. Kasai, S. Shimizu, Y. Tatara, J. Mimura, K. Itoh, Regulation of Nrf2 by mitochondrial reactive oxygen species in physiology and pathology, Biomolecules 10 (2) (2020).
[54] S. Kovac, P.R. Angelova, K.M. Holmstrom, Y. Zhang, A.T. Dinkova-Kostova, A. Y. Abramov, Nrf2 regulates ROS production by mitochondria and NADPH oxidase, Biochim. Biophys. Acta 1850 (4) (2015) 794–801.
[55] K.I. Tong, A. Kobayashi, F. Katsuoka, M. Yamamoto, Two-site substrate recognition model for the Keap1-Nrf2 system: a hinge and latch mechanism, Biol. Chem. 387 (10–11) (2006) 1311–1320.
[56] X. Wang, X. Zhang, E.S.H. Chu, X. Chen, W. Kang, F. Wu, et al., Defective lysosomal clearance of autophagosomes and its clinical implications in nonalcoholic steatohepatitis, Faseb. J. 32 (1) (2018) 37–51.
[57] H. Fukushima, S. Yamashina, A. Arakawa, G. Taniguchi, T. Aoyama, A. Uchiyama, et al., Formation of p62-positive inclusion body is associated with macrophage polarization in non-alcoholic fatty liver disease, Hepatol. Res. 48 (9) (2018) 757–767.
[58] J.S. Park, S.Y. Oh, D.H. Lee, Y.S. Lee, S.H. Sung, H.W. Ji, et al., p62/SQSTM1 is required for the protection against endoplasmic reticulum stress-induced apoptotic cell death, Free Radic. Res. 50 (12) (2016) 1408–1421.
[59] A. Jain, T. Lamark, E. Sjottem, K.B. Larsen, J.A. Awuh, A. Overvatn, et al., p62/SQSTM1 is a target gene for transcription factor NRF2 and creates a positive feedback loop by inducing antioxidant response element-driven gene transcription, J. Biol. Chem. 285 (29) (2010) 22576–22591.
[60] K. Taniguchi, S. Yamachika, F. He, M. Karin, p62/SQSTM1-Dr. Jekyll and Mr. Hyde that prevents oxidative stress but promotes liver cancer, FEBS Lett. 590 (15) (2016) 2375–2397.
[61] K. Hashimoto, A.N. Simmons, R. Kajino-Sakamoto, Y. Tsuji, J. Ninomiya-Tsuji, TAK1 regulates the Nrf2 antioxidant system through modulating p62/SQSTM1, Antioxidants Redox Signal. 25 (17) (2016) 953–964.
[62] J.Y. Park, H.Y. Sohn, Y.H. Koh, C. Jo, Curcumin activates Nrf2 through PKCdelta-mediated p62 phosphorylation at Ser351, Sci. Rep. 11 (1) (2021) 8430.
[63] A. Almanza, A. Carlesso, C. Chintha, S. Creedican, D. Doultsinos, B. Leuzzi, et al., Endoplasmic reticulum stress signalling - from basic mechanisms to clinical applications, FEBS J. 286 (2) (2019) 241–278.
[64] S.B. Cullinan, D. Zhang, M. Hannink, E. Arvisais, R.J. Kaufman, J.A. Diehl, Nrf2 is a direct PERK substrate and effector of PERK-dependent cell survival, Mol. Cell Biol. 23 (20) (2003) 7198–7209.
[65] S.B. Cullinan, J.A. Diehl, PERK-dependent activation of Nrf2 contributes to redox homeostasis and cell survival following endoplasmic reticulum stress, J. Biol. Chem. 279 (19) (2004) 20108–20117.
[66] C.H. He, P. Gong, B. Hu, D. Stewart, M.E. Choi, A.M. Choi, et al., Identification of activating transcription factor 4 (ATF4) as an Nrf2-interacting protein. Implication for heme oxygenase-1 gene regulation, J. Biol. Chem. 276 (24) (2001) 20858–20865.
[67] W. B'Chir, A.C. Maurin, V. Carraro, J. Averous, C. Jousse, Y. Muranishi, et al., The eIF2alpha/ATF4 pathway is essential for stress-induced autophagy gene expression, Nucleic Acids Res. 41 (16) (2013) 7683–7699.
[68] J. Han, S.H. Back, J. Hur, Y.H. Lin, R. Gildersleeve, J. Shan, et al., ER-stress-induced transcriptional regulation increases protein synthesis leading to cell death, Nat. Cell Biol. 15 (5) (2013) 481–490.
[69] C. Liu, D.Y. Yan, C. Wang, Z. Ma, Y. Deng, W. Liu, et al., Manganese activates autophagy to alleviate endoplasmic reticulum stress-induced apoptosis via PERK pathway, J. Cell Mol. Med. 24 (1) (2020) 328–341.
[70] M. Luhr, M.L. Torgersen, P. Szalai, A. Hashim, A. Brech, J. Staerk, et al., The kinase PERK and the transcription factor ATF4 play distinct and essential roles in autophagy resulting from tunicamycin-induced ER stress, J. Biol. Chem. 294 (20) (2019) 8197–8217.
[71] C. Sarcinelli, H. Dragic, M. Piecyk, V. Barbet, C. Duret, A. Barthelaix, et al., ATF4-Dependent NRF2 transcriptional regulation promotes antioxidant protection during endoplasmic reticulum stress, Cancers 12 (3) (2020).
[72] W. Quan, M.S. Lee, Role of autophagy in the control of body metabolism, Endocrinol. Metab. (Seoul) 28 (1) (2013) 6–11.
[73] S.H. Kim, G. Kim, D.H. Han, M. Lee, I. Kim, B. Kim, et al., Ezetimibe ameliorates steatohepatitis via AMP activated protein kinase-TFEB-mediated activation of autophagy and NLRP3 inflammasome inhibition, Autophagy 13 (10) (2017) 1767–1781.
[74] B. Liu, X. Deng, Q. Jiang, G. Li, J. Zhang, N. Zhang, et al., Scoparone improves hepatic inflammation and autophagy in mice with nonalcoholic steatohepatitis by regulating the ROS/P38/Nrf2 axis and PI3K/AKT/mTOR pathway in macrophages, Biomed. Pharmacother. 125 (2020) 109895.
[75] T. Hidvegi, M. Ewing, P. Hale, C. Dippold, C. Beckett, C. Kemp, et al., An autophagy-enhancing drug promotes degradation of mutant alpha1-antitrypsin Z and reduces hepatic fibrosis, Science 329 (5988) (2010) 229–232.
[76] A.U. Nissar, L. Sharma, M.A. Mudasir, L.A. Nazir, S.A. Umar, P.R. Sharma, et al., Chemical chaperone 4-phenyl butyric acid (4-PBA) reduces hepatocellular lipid

accumulation and lipotoxicity through induction of autophagy, J. Lipid Res. 58 (9) (2017) 1855–1868.
[77] J. Kim, K.L. Guan, Regulation of the autophagy initiating kinase ULK1 by nutrients: roles of mTORC1 and AMPK, Cell Cycle 10 (9) (2011) 1337–1338.
[78] M. Zhao, D.J. Klionsky, AMPK-dependent phosphorylation of ULK1 induces autophagy, Cell Metabol. 13 (2) (2011) 119–120.
[79] B. Meusser, C. Hirsch, E. Jarosch, T. Sommer, ERAD: the long road to destruction, Nat. Cell Biol. 7 (8) (2005) 766–772.
[80] W. Zheng, W. Xie, D. Yin, R. Luo, M. Liu, F. Guo, ATG5 and ATG7 induced autophagy interplays with UPR via PERK signaling, Cell Commun. Signal. 17 (1) (2019) 42.
[81] A. Henkel, R.M. Green, The unfolded protein response in fatty liver disease, Semin. Liver Dis. 33 (4) (2013) 321–329.
[82] J.H. Lin, P. Walter, T.S. Yen, Endoplasmic reticulum stress in disease pathogenesis, Annu. Rev. Pathol. 3 (2008) 399–425.